Summer 2019

Unconditionally Energy Stable Linear Schemes for a Two-Phase Diffuse Interface Model with Peng-Robinson Equation of State

Chenfei Zhang

Unconditionally energy stable linear schemes for a two-phase diffuse interface model with Peng-Robinson equation of state

by

Chenfei Zhang

Bachelor of Science
University of Science and Technology of China, 2012

Master of Science
University of Science and Technology of China, 2014

Submitted in Partial Fulfillment of the Requirements

for the Degree of Doctor of Philosophy in

Mathematics

College of Arts and Sciences

University of South Carolina

2019

Accepted by:

Lili Ju, Major Professor

Zhu Wang, Major Professor

Yi Sun, Committee Member

Xinfeng Liu, Committee Member

Chen Li, Committee Member

Cheryl L. Addy, Vice Provost and Dean of the Graduate School

Acknowledgments

First and foremost, I would like to express my deepest appreciation for my advisor Dr. Lili Ju and co-advisor Dr. Zhu Wang, who mentored me closely in my work and guided me towards completion of my studies. They offered lots of valuable advice and instructions in our weekly group meetings and without their guidance and persistent help this dissertation would not have been possible.

I am extremely grateful to Dr. Hongwei Li from Shandong Normal University, who offered advice in general and helped answer specific questions in the development of this dissertation. I also would like to extend my gratitude to my committee members Dr. Yi Sun, Dr. Xinfeng Liu and Dr. Chen Li for extending their knowledge in the classroom and for their enthusiasm towards research. Many thanks to all of my professors and colleagues, many of them supported me during my graduate studies in University of South Carolina.

Finally I would like to thank my family for helping and believing in me by all means. They are the ones supporting me and never letting me down. Special thanks to my wife, Coco. She has continually supported and encouraged me all the time. She cheers for me when things go well, and picks me up when things fall apart. Without her, I would never have come this far.

Abstract

Many problems in the fields of science and engineering, particularly in materials science and fluid dynamic, involve flows with multiple phases and components. From mathematical modeling point of view, it is a challenge to perform numerical simulations of multiphase flows and study interfaces between phases, due to the topological changes, inherent nonlinearities and complexities of dealing with moving interfaces.

In this work, we investigate numerical solutions of a diffuse interface model with Peng-Robinson equation of state. Based on the invariant energy quadratization approach, we develop first and second order time stepping schemes to solve the liquid-gas diffuse interface problems for both pure substances and their mixtures. The resulting temporal semi-discretizations from both schemes lead to linear systems that are symmetric and positive definite at each time step, therefore they can be numerically solved by many efficient linear solvers. The unconditional energy stabilities in the discrete sense are rigorously proven, and various numerical simulations in two and three dimensional spaces are presented to validate the accuracies and stabilities of the proposed linear schemes.

Table of Contents

List of Figures

Chapter 1

INTRODUCTION

Subsurface flow often involves multiple fluid phases, and the phenomena of subsurfaces often allow for the mixing of immiscible and partially miscible fluids. A typical well-known application is the subsurface oil and gas reservoir, which contains oil phase, gas phase and water phase, together with the solid phase (soil or rock) [15]. There have been many efforts to study multiphase fluids, especially in reservoir engineering [50, 46, 47, 22, 36, 53]. In addition to oil reservoir management, modeling and understanding multiphase systems are also crucial to many environment issues [48]. It is highly important to model and numerically simulate these interfaces between phases to understand physical phenomena, such as liquid droplets, gas bubbles, and capillary pressures.

At least three methodologies have been proposed to model the interfaces between phases. Based on the molecular scale, the first approach is to model it by applying the molecular dynamics simulation or the molecular Monte Carlo simulation with a given intermolecular potential function (e.g., Lennard-Jones potential) [7, 18]. Although this method can describe the interfaces in detail, the central processing unit intensive property limits its application to a small part of simple substances. The second approach is interface tracking (sharp interface modeling [42], front-tracking [19], immersed boundary [43]) where the interface is modeled by a zero-thickness two-dimensional entity [42]. Assuming that the interface tension is given, this approach can be successfully applied to predict the shape and dynamics of the interface. However, it can not provide information within the interface itself. The third methodology

is to use phase field model (interface capturing, diffuse interface theory) to simulate multiphase and multi-component flows [1, 2, 12, 13, 35, 40], which is an increasingly popular choice for modeling the motion of multiphase and multi-component fluids. In the phase field model, a conserved order parameter such as a mass concentration that varies continuously over thin interfacial layers is introduced, and the order parameter is mostly uniform in the bulk phases. Based on this idea, sharp fluid interfaces are replaced by thin but nonzero thickness transition regions where the interfacial forces are smoothly distributed. The free interface can be automatically tracked without imposing any mathematical conditions on the moving interface. One advantage of the phase field model is that the governing system of equations in the model can be derived from the variational principle. Moreover, the phase field model usually leads to well-posed nonlinear systems that satisfy the energy dissipation law. Therefore, this model has become a well-known simulation tool to resolve the motion of free interfaces in multiple components, and has also been successfully applied to many problems in the fields of science and industry [5, 21, 24, 25, 49, 51, 52].

In order to study the interface between phases, the development of energy stable schemes for phase field model is an important issue. There are several popular numerical approaches to construct energy stable schemes. The first approach is the convex splitting method, which is introduced by Elliott and Stuart [6, 14] and popularized by Eyre [11]. The main idea is assuming the free energy density can be split as the difference of two convex functions, where the convex part is treated implicitly and the concave part is treated explicitly. Although the convex splitting method is unconditionally energy stable and uniquely solvable, it reduces to a nonlinear system at each time step and the implementation is complicated and the computational cost is high. The second widely used approach is the stabilized method which treats the nonlinear terms explicitly, and adds an artificial stabilization term to overcome strict temporal step constraint [62, 63]. This method is also energy stable and produces a

linear system at each time step which is easy to implement. However, it is not easy to find the stabilization term for all problems, and it can not be unconditionally energy stable for second order scheme.

In this dissertation, we focus on the diffuse interface modeling of both single-component and multi-component two-phase fluid systems, and consider the energy stable schemes for a more realistic model with Peng-Robinson equation of state. The Peng-Robinson equation of state, as a diffuse interface model to describe the real states of hydrocarbon fluids in the petroleum industry, has become one of the most useful and successfully applied models for thermodynamic and volumetric calculations in both industrial and academic fields [34, 41]. It has been considered as one of the best two constants third degree equations of state applicable to vapor-liquid equilibria, volumetric and thermodynamic properties calculations for pure substances and mixtures. The structure of its energy functional is highly nonlinear and more complicated than many conventional phase field models. Therefore, the development of accurate, efficient, easy-to-implement, and energy stable numerical schemes is a very important and challenging issue. Many efforts have been devoted to designing numerical schemes with energy stability. Qiao and Sun developed an efficient scheme for single-component systems with Peng-Robinson equation of state [40]. They established a clean convex splitting of the total Helmholtz free energy and treated the convex and concave parts separately. However, it is not straightforward to extend the convex splitting method from single-component to multi-component systems. Fan and his collaborators designed a component-wise convex splitting scheme for diffuse interface models with Peng-Robinson equation of state [17]. Kou and Sun proposed a modified Newton's method to solve the nonlinear model and proved the maximum principle of the molar density for multi-component systems [26]. Some recent developments in numerical algorithms for the multi-component diffuse interface model with Peng-Robinson equation of state can be referenced to [25, 27, 31, 29, 30].

In this work, we are devoted to designing efficient linear unconditionally energy stable numerical schemes to solve single and multiple components diffuse interface model with Peng-Robinson equation of state. Combining the stabilized method, the Invariant Energy Quadratization (IEQ) approach, which is a novel method and applicable to a large class of free energies, is adopted to develop the numerical schemes for Peng-Robinson equation of state. Yang and his collaborators designed the IEQ approach by generalizing the Lagrange multiplier approach, and many phase field models have been solved by this approach [54, 55, 56, 57, 58, 59, 61]. The main idea of the IEQ method is to transform the free energy into a quadratic form with a set of auxiliary variables. A new but equivalent system is obtained, which still retains the energy dissipation law in terms of the auxiliary variables. This approach enjoys the following advantages: (i) all nonlinear terms in the new system can be discretized by semi-explicit schemes in time to produce a linear system at each time step so it is very efficient; (ii) the energy dissipation laws in the discrete sense are preserved; (iii) it can be easily extended to higher-order schemes. Moreover, the operator of obtained linear system is symmetric positive definite and it can be numerically solved by many efficient linear solvers such as preconditioned CG or other Krylov subspace methods.

The rest of this dissertation is organized as follows. In Chapter 2, we briefly review the diffuse interface model with Peng-Robinson equation of state. In Chapter 3 and Chapter 4, we derive the gradient flow problems associated with this model based on the IEQ approach, and develop linear first and second order time stepping schemes for both single-component and multi-component systems. We prove the well-posedness of the systems and unconditional energy stabilities. In Chapter 5, we present two and three dimensional numerical simulations to validate the accuracies and stabilities of the proposed linear schemes for both systems. Finally some concluding remarks and future work are given in Chapter 6.

Chapter 2

Mathematical Modeling

2.1 Diffuse interface model from gradient theory

A fluid system consisting of a fixed number of species on a fixed domain Ω with a spatially uniform-distributed given temperature is considered. The total Helmholtz free energy achieves a global minimum at the equilibrium state, according to the second law of thermodynamics [3]. We are interested in the equilibrium state of the system in this work.

We denote by M the number of components in the fluid mixture and n_i the molar concentration of the component i. Let $\mathbf{n} = (n_1, n_2, \cdots, n_M)^T$ be the molar concentrations of all components and $n = n_1 + n_2 + \cdots + n_M$ be the molar density of the fluid. According to the gradient theory, one of the most popular thermodynamic theories for inhomogeneous fluid, the total Helmholtz energy density has two contributions, one from the thermodynamic theory of homogeneous fluids and the other one from inhomogeneity of the fluid. That is

$$F(\mathbf{n}) = \int_\Omega f(\mathbf{n}; T) d\mathbf{x} = F_0(\mathbf{n}; T, \Omega) + F_\nabla(\mathbf{n}; T, \Omega) = \int_\Omega f_0(\mathbf{n}; T) d\mathbf{x} + \int_\Omega f_\nabla(\mathbf{n}; T) d\mathbf{x}, \tag{2.1}$$

where T is the temperature, $F_0(\mathbf{n}; T, \Omega)$ is the contribution of Helmholtz free energy density from the homogeneous fluid theory, and the $F_\nabla(\mathbf{n}; T, \Omega)$ is the contribution of Helmholtz free energy density from the concentration gradient. The inhomogeneous term or the gradient contribution $f_\nabla(\mathbf{n}; T)$ can be modeled by a simple quadratic

relation

$$f_{\nabla}(\mathbf{n};T) = \frac{1}{2}\sum_{i,j=1}^{M} c_{ij}\nabla n_i \cdot \nabla n_j,$$

where c_{ij} is the influence parameter. The parameter c_{ij} is a function of molar concentrations and temperature. The influence parameter depends on molar concentrations only weakly, thus it is often justified to assume that c_{ij} is a constant for a given fixed temperature T.

Since the molar concentration $\mathbf{n}$ at equilibrium minimizes the total Helmholtz free energy F for a closed and conserved fluid system with temperature T, the mathematical statement of the problem is formulated as follows: find $\mathbf{n}^* \in H$ satisfying

$$F(\mathbf{n}^*) = \min_{\mathbf{n}\in H} F(\mathbf{n}), \tag{2.2}$$

subject to the constraint

$$\int_{\Omega} \mathbf{n} d\mathbf{x} = \mathbf{N}, \tag{2.3}$$

where H be a space of functions with certain regularity, $\mathbf{N} = (N_1, N_2, \cdots, N_M)^T$ is a given constant vector representing the fixed amount of material mass for each component in the system.

2.2 A more realistic model with Peng-Robinson equation of state

The Peng-Robinson equation of state is the most popular model for computing the fluid equilibrium property of petroleum fluids in reservoir engineering and oil industries, since its publication in 1976. We briefly review the Peng-Robinson equation of state in this section.

2.2.1 Model with Peng-Robinson equation of state

The Helmholtz free energy $f_0(\mathbf{n})$ of a homogeneous fluid in the diffuse interface model with Peng-Robinson equation of state is given by

$$f_0(\mathbf{n};T) = f_{01}(\mathbf{n}) + f_{02}(\mathbf{n}), \tag{2.4}$$

with

$$f_{01}(\mathbf{n}) = RT\sum_{i=1}^{M} n_i(\ln n_i - 1) - nRT\ln(1-bn), \tag{2.5}$$

$$f_{02}(\mathbf{n}) = \frac{a(T)n}{2\sqrt{2}b}\ln(\frac{1+(1-\sqrt{2})bn}{1+(1+\sqrt{2})bn}), \tag{2.6}$$

where T is the temperature of the mixture and R is the universal gas constant and $n = \sum_{i=1}^{M} n_i$.

2.2.2 Parameters

The two parameters, energy parameter a which depends on temperature T, and the co-volume parameter b, are utilized in the Peng-Robinson equation of state. All can be found in [39, 25, 26, 31, 40] and the references cited therein. The universal gas constant R has a value of approximately $8.31432\text{JK}^{-1}\text{mol}^{-1}$, and the temperature-dependent energy parameter a and the co-volume parameter b in the Peng-Robinson equation of state are defined as

$$a(T) = \sum_{i=1}^{M}\sum_{j=1}^{M}(1-k_{ij})y_i y_j\sqrt{a_i(T)a_j(T)}, \qquad b = \sum_{i=1}^{M} y_i b_i,$$

with $y_i = \dfrac{n_i}{n}$ being the mole fraction of component i. The binary interaction coefficient $0 \le k_{ij} \le 1$ is assumed to be a constant for a fixed species pair and usually computed from experimental correlation [38]. The Peng-Robinson parameters for the pure-substance component i, a_i and b_i, are calculated from the critical properties of the specie

$$\begin{aligned} a_i(T) &= 0.45724\frac{R^2T_{c_i}^2}{P_{c_i}}\left(1+m_i\left(1-\sqrt{\frac{T}{T_{c_i}}}\right)\right)^2, \\ b_i &= 0.07780\frac{RT_{c_i}}{P_{c_i}}, \end{aligned}$$

where T_{c_i} and P_{c_i} represent the critical temperature and pressure of the pure substance component i respectively, which are intrinsic properties of the specie and available for

most substances encountered in engineering applications. The parameter m_i for modeling the influence of temperature on a_i is experimentally correlated to the acentric parameter of the specie ω_i by

$$m_i = \begin{cases} 0.37464 \quad + 1.54226\omega_i \quad - 0.26992\omega_i^2, & \omega_i \leq 0.49, \\ 0.379642 + 1.485030\omega_i - 0.164423\omega_i^2 + 0.016666\omega_i^3, & \omega_i > 0.49, \end{cases}$$

with

$$\omega_i = \frac{3}{7}\left(\frac{\log_{10}(\frac{P_{c_i}}{14.695\ \text{PSI}})}{\frac{T_{c_i}}{T_{b_i}} - 1}\right) - 1 = \frac{3}{7}\left(\frac{\log_{10}(\frac{P_{c_i}}{1\ \text{atm}})}{\frac{T_{c_i}}{T_{b_i}} - 1}\right) - 1,$$

where T_{b_i} represents the normal boiling point of the pure substance i, "PSI" is "pounds per square inch", and "atm" refers to the standard atmosphere pressure (equal to 101325Pa).

The dependence of influence parameter c_{ij} on the molar concentrations is in practice very weak, and it is common to assume that $c_{ij} = c_{ij}(T)$ is just a temperature-dependent parameter, which can be obtained by adopting the modified geometric mean

$$c_{ij}(T) = (1 - \beta_{ij})\sqrt{c_i(T)c_j(T)}.$$

Note β_{ij} is the binary interaction coefficient for the influence parameter, usually required to be included between 0 and 1 and $\beta_{ij} = \beta_{ji}$ to maintain the stability of the interfaces, and c_i is the influence parameter of the pure substance component i, computed by

$$c_i = a_i b_i^{\frac{2}{3}}\left(m_{1,i}^c\left(1 - \frac{T}{T_{c_i}}\right) + m_{2,i}^c\right),$$

with $m_{1,i}^c$ and $m_{2,i}^c$ being the coefficients correlated merely with the acentric factor ω_i by

$$m_{1,i}^c = -\frac{10^{-16}}{1.2326 + 1.3757\omega_i}, \qquad m_{2,i}^c = \frac{10^{-16}}{0.9051 + 1.5410\omega_i}.$$

Chapter 3

Numerical schemes for single-component system

In this chapter, we will focus our study on a single-component system with $M = 1$, that is, a system with only pure substance. We will design first and second order numerical time stepping schemes to solve the diffuse interface model problem with Peng-Robinson equation of state for such system.

3.1 Single-component system

Our model can be simplified to the following minimization problem: Find n satisfying

$$\min_n F(n) = \int_\Omega (f_0(n) + f_\nabla(n))\, d\mathbf{x}, \tag{3.1}$$

subject to

$$\int_\Omega n\, d\mathbf{x} = N, \tag{3.2}$$

where $f_\nabla(n) = \dfrac{c}{2}\nabla n \cdot \nabla n$ and $f_0(n) = f_{01}(n) + f_{02}(n)$ with

$$f_{01}(n) = RTn(\ln n - 1) - nRT\ln(1 - bn),$$

and

$$f_{02}(n) = \frac{a(T)n}{2\sqrt{2}b}\ln\left(\frac{1 + (1 - \sqrt{2})bn}{1 + (1 + \sqrt{2})bn}\right).$$

3.1.1 Invariant energy quadratization

We define the total material mass for the component in the system as $U(n) = \int_\Omega n\, d\mathbf{x}$, which should be fixed according to the constraint (3.2). We next transform the con-

strained minimization problem (3.1) and (3.2) to the following unconstrained minimization problem

$$\min_n E(n) = \int_\Omega \left(\frac{c}{2}|\nabla n|^2 + f_0(n) \right) d\mathbf{x} + \frac{P}{2}(U(n) - N)^2, \tag{3.3}$$

where $P > 0$ is a suitable constant penalty parameter. It is clear that $f_0(n)$ is bounded from below, although it is not always positive in the whole domain. To use the IEQ method proposed in [54, 56, 57, 58, 55, 61, 59], we rewrite the free energy functional in (3.3) to the following form:

$$E(n) = \int_\Omega \left(\frac{c}{2}|\nabla n|^2 + \left(\sqrt{f_0(n) + B_0} \right)^2 - B_0 \right) d\mathbf{x} + \frac{P}{2}(U(n) - N)^2, \tag{3.4}$$

where B_0 is a positive constant to ensure $f_0(n) + B_0 > 0$. We emphasize that the free energy is invariant because we simply add a zero term therein. Next we define two auxiliary variables to be the square roots of $f_0(n) + B_0$ and $(U(n) - N)^2$ respectively as

$$W = \sqrt{f_0(n) + B_0}, \tag{3.5}$$

$$V = U(n) - N. \tag{3.6}$$

Then the free energy functional (3.4) can be expressed as the following new but equivalent functional

$$E(n, W, V) = \int_\Omega \left(\frac{c}{2}|\nabla n|^2 + W^2 - B_0 \right) d\mathbf{x} + \frac{P}{2}V^2. \tag{3.7}$$

3.1.2 Energy dissipation law

Based on the variational approach, the governing dynamical equation for $n(\mathbf{x}, t)$ is given by

$$n_t = -\frac{\delta E(n)}{\delta n} = c\Delta n - WH(n) - PV, \tag{3.8}$$

where $H(n) = \dfrac{f_0'(n)}{\sqrt{f_0(n)+B_0}}$. We obtain a system of evolution equations of the variables n, W, V as follows

$$\begin{cases} n_t = c\Delta n - WH(n) - PV, & (3.9) \\ W_t = \dfrac{1}{2}H(n)n_t, & (3.10) \\ V_t = \displaystyle\int_\Omega n_t \, d\mathbf{x}. & (3.11) \end{cases}$$

According to the theory of gradient flow, the steady state solutions of the above partial differential equation system (3.9)-(3.11) will give us local minimizers of (3.7) and thus of (3.3). We finally close the system (3.9)-(3.11) by adding the periodic boundary (or the no-flux) condition and the following compatible initial condition:

$$n|_{(t=0)} = n_0, \quad W|_{(t=0)} = \sqrt{f_0(n_0)+B_0}, \quad V|_{(t=0)} = 0. \tag{3.12}$$

Denote by $(h(\mathbf{x}), g(\mathbf{x})) = \displaystyle\int_\Omega h(\mathbf{x})g(\mathbf{x})d\mathbf{x}$ the L^2 inner product of any two functions $h(\mathbf{x})$ and $g(\mathbf{x})$, and by $\|g\| = \sqrt{(g,g)}$ the L^2 norm of the function $g(\mathbf{x})$. Taking the L^2 inner product of (3.9) with n_t, of (3.10) with W, and taking the simple multiplication of (3.11) with PV, we have

$$\begin{cases} (n_t, n_t) = c(\Delta n, n_t) - (WH(n), n_t) - (PV, n_t), & (3.13) \\ (W_t, W) = \dfrac{1}{2}(H(n)n_t, W), & (3.14) \\ PVV_t = P(V, V_t). & (3.15) \end{cases}$$

Summing (3.13)-(3.15) up, we get the energy dissipation law of the system (3.9)-(3.11) as

$$\frac{d}{dt}E(n, W, V) = -\|n_t\|^2 \leq 0. \tag{3.16}$$

3.2 Numerical schemes for time integration

In this section, we will focus on designing numerical schemes for time discretization of the system (3.9)-(3.11), that lead to linear systems with self-adjoint positive definite spatial operators at each time step, and satisfy discrete analogues of the energy disspation law (3.16).

3.2.1 First order scheme

Let $\delta t > 0$ denote the time step size and set $t^k = k\delta t$ for $0 \le k \le K$ with the ending time $T = K\delta t$. Assuming that n^k, W^k and V^k are already calculated, we then compute n^{k+1}, W^{k+1} and V^{k+1} from the following temporally semi-discretized system

$$\begin{cases} \dfrac{n^{k+1}-n^k}{\delta t} = c\Delta n^{k+1} - W^{k+1}H(n^k) - PV^{k+1}, & (3.17) \\ \dfrac{W^{k+1}-W^k}{\delta t} = \dfrac{1}{2}H(n^k)\dfrac{n^{k+1}-n^k}{\delta t}, & (3.18) \\ \dfrac{V^{k+1}-V^k}{\delta t} = \displaystyle\int_\Omega \frac{n^{k+1}-n^k}{\delta t}\, d\mathbf{x}, & (3.19) \end{cases}$$

with the periodic boundary condition. We note that (3.18) and (3.19) can be rewritten as

$$W^{k+1} = W^k - \frac{1}{2}H(n^k)n^k + \frac{1}{2}H(n^k)n^{k+1} = A_1 + A_2(n^{k+1}), \tag{3.20}$$

$$V^{k+1} = V^k - \int_\Omega n^k\, d\mathbf{x} + \int_\Omega n^{k+1}\, d\mathbf{x} = A_3 + A_4(n^{k+1}), \tag{3.21}$$

where

$$A_1 = W^k - \frac{1}{2}H(n^k)n^k, \quad A_2(n) = \frac{1}{2}H(n^k)n,$$
$$A_3 = V^k - \int_\Omega n^k\, d\mathbf{x}, \qquad A_4(n) = \int_\Omega n\, d\mathbf{x}.$$

Thus, (3.17) can be rewritten as the reduced linear system

$$\frac{n^{k+1}}{\delta t} - c\Delta n^{k+1} + H(n^k)A_2(n^{k+1}) + PA_4(n^{k+1}) = \frac{n^k}{\delta t} - H(n^k)A_1 - PA_3. \tag{3.22}$$

The linear system (3.22) can be expressed as $\mathbb{A}n^{k+1} = b$, and we need solve for n^{k+1} from it.

Theorem 3.1. *The linear spatial operator $\mathbb{A}$ is symmetric positive definite.*

Proof. It is not hard to verify that

$$\begin{aligned} (\mathbb{A}n, \varphi) &= \frac{1}{\delta t}(n,\varphi) - c(\Delta n, \varphi) + H(n^k)(A_2(n),\varphi) + P(A_4(n),\varphi) \\ &= \frac{1}{\delta t}(\varphi.n) - c(n, \Delta\varphi) + H(n^k)(n, A_2(\varphi)) + PA_4(n)A_4(\varphi) \\ &= (n, \mathbb{A}\varphi), \end{aligned}$$

and

$$(\mathbb{A}n, n) = \frac{1}{\delta t}(n, n) - c(\Delta n, n) + H(n^k)(A_2(n), n) + P(A_4(n), n) \geq \frac{1}{\delta t}||n||^2.$$

Therefore, the operator $\mathbb{A}$ is symmetric positive definite. □

Let us define $\|n\|_{\mathbb{A}} = \sqrt{(\mathbb{A}n, n)}$ for any $n \in L^2_{per}(\Omega)$ and the subset $\mathbf{X} = \{n \in L^2_{per}(\Omega) : \|n\|_{\mathbb{A}} < \infty\}$, where $L^2_{per}(\Omega)$ denotes the subspace of all functions $n \in L^2(\Omega)$ with the periodic or no-flux boundary conditions. It is easy to show that $\|n\|_{\mathbb{A}}$ is a norm for $L^2_{per}(\Omega)$ and $\mathbf{X}$ is a Hilbert subspace associated with the norm $\|n\|_{\mathbb{A}}$. The well-posedness of the linear system $\mathbb{A}n = b$ in the weak sense comes from the Lax-Milgram theorem, i.e., the linear system (3.22) admits a unique weak solution in $\mathbf{X}$.

Theorem 3.2. *The first order linear system (3.17)-(3.19) is unconditionally energy stable, that is, it satisfies the following discrete energy dissipation law*

$$E^{k+1}_{1st} \leq E^k_{1st} - \frac{\left\|n^{k+1} - n^k\right\|^2}{\delta t}, \tag{3.23}$$

where

$$E^k_{1st} = \frac{c}{2}\left\|\nabla n^k\right\|^2 + \left\|W^k\right\|^2 + \frac{P}{2}(V^k)^2.$$

Proof. By taking the L^2 inner product of (3.17) with $n^{k+1} - n^k$, we have

$$\frac{1}{\delta t}\left\|n^{k+1} - n^k\right\|^2 = c(\Delta n^{k+1}, n^{k+1} - n^k) - (H(n^k)W^{k+1}, n^{k+1} - n^k) - P(V^{k+1}, n^{k+1} - n^k). \tag{3.24}$$

By taking the L^2 inner product of (3.18) with W^{k+1} and applying the following identities

$$2(a - b, a) = |a|^2 - |b|^2 + |a - b|^2, \tag{3.25}$$

we obtain

$$\left\|W^{k+1}\right\|^2 - \left\|W^k\right\|^2 + \left\|W^{k+1} - W^k\right\|^2 = (H(n^k)W^{k+1}, n^{k+1} - n^k). \tag{3.26}$$

By taking the simple multiplication of (3.19) with PV^{k+1} and applying (3.25), we have

$$\frac{P}{2}((V^{k+1})^2-(V^k)^2+(V^{k+1}-V^k)^2)=P(V^{k+1},n^{k+1}-n^k). \tag{3.27}$$

Combination of (3.24)-(3.27) gives us

$$\begin{aligned}&\frac{c}{2}\Big(\left\|\nabla n^{k+1}\right\|^2-\left\|\nabla n^k\right\|^2+\left\|\nabla n^{k+1}-\nabla n^k\right\|^2\Big)+\Big(\left\|W^{k+1}\right\|^2-\left\|W^k\right\|^2\\&+\left\|W^{k+1}-W^k\right\|^2\Big)+\frac{P}{2}((V^{k+1})^2-(V^k)^2+(V^{k+1}-V^k)^2)=-\frac{1}{\delta t}\left\|n^{k+1}-n^k\right\|^2,\end{aligned}$$

and thus

$$\begin{aligned}&\frac{c}{2}\Big(\left\|\nabla n^{k+1}\right\|^2+\left\|\nabla n^{k+1}-\nabla n^k\right\|^2\Big)+\Big(\left\|W^{k+1}\right\|^2+\left\|W^{k+1}-W^k\right\|^2\Big)+\frac{P}{2}((V^{k+1})^2\\&+(V^{k+1}-V^k)^2)=\frac{c}{2}\left\|\nabla n^k\right\|^2+\left\|W^k\right\|^2+\frac{P}{2}(V^k)^2-\frac{1}{\delta t}\left\|n^{k+1}-n^k\right\|^2.\end{aligned} \tag{3.28}$$

After dropping some positive terms from above equation (3.28), we have the discrete energy laws (3.23). □

3.2.2 Second order scheme

Based on the second order backward differentiation formulas (BDF2), assuming that we have found n^{k-1}, W^{k-1}, V^{k-1} and n^k, W^k, V^k, we then compute n^{k+1}, W^{k+1} and V^{k+1} as follows

$$\begin{cases}\dfrac{3n^{k+1}-4n^k+n^{k-1}}{2\delta t}=c\Delta n^{k+1}-H(n^*)W^{k+1}-PV^{k+1}, & (3.29)\\[2ex] \dfrac{3W^{k+1}-4W^k+W^{k-1}}{2\delta t}=\dfrac{1}{2}H(n^*)\dfrac{3n^{k+1}-4n^k+n^{k-1}}{2\delta t}, & (3.30)\\[2ex] \dfrac{3V^{k+1}-4V^k+V^{k-1}}{2\delta t}=\displaystyle\int_\Omega\frac{3n^{k+1}-4n^k+n^{k-1}}{2\delta t}\,d\mathbf{x}, & (3.31)\end{cases}$$

where $n^*=2n^k-n^{k-1}$. For (3.30)-(3.31), we have

$$\begin{aligned}W^{k+1}=&\frac{4W^k-W^{k-1}}{3}-\frac{1}{2}H(n^*)\frac{4n^k-n^{k-1}}{3}+\frac{1}{2}H(n^*)n^{k+1},\\V^{k+1}=&\frac{4V^k-V^{k-1}}{3}-\int_\Omega\frac{4n^k-n^{k-1}}{3}\,d\mathbf{x}+\int_\Omega n^{k+1}\,d\mathbf{x}.\end{aligned}$$

Set

$$B_1 = W^+ - \frac{1}{2}H(n^*)n^+, \qquad B_2(n) = \frac{1}{2}H(n^*)n,$$
$$B_3 = V^+ - \int_\Omega n^+ \, d\mathbf{x}, \qquad B_4(n) = \int_\Omega n \, d\mathbf{x},$$

where $S^+ = \frac{4S^k - S^{k-1}}{3}$. Thus, we obtain

$$W^{k+1} = B_1 + B_2(n^{k+1}), \qquad V^{k+1} = B_3 + B_4(n^{k+1}).$$

In turn, we have the following reduced linear system

$$\begin{aligned}&\frac{3}{2\delta t}n^{k+1} - c\Delta n^{k+1} + H(n^*)B_2(n^{k+1}) + PB_4(n^{k+1})\\ &= \frac{1}{2\delta t}(4n^k - n^{k-1}) - H(n^*)B_1 - PB_3.\end{aligned}$$

The above linear system can be expressed as $\hat{\mathbb{A}}n^{k+1} = \hat{b}$, and we need solve for n^{k+1} from it.

Theorem 3.3. *The linear spatial operator $\hat{\mathbb{A}}$ is symmetric positive definite.*

Proof. We can verify that

$$\begin{aligned}(\hat{\mathbb{A}}n, \varphi) &= \frac{3}{2\delta t}(n, \varphi) - c(\Delta n, \varphi) + H(n^*)(B_2(n), \varphi) + P(B_4(n), \varphi)\\ &= \frac{3}{2\delta t}(\varphi, n) - c(n, \Delta\varphi) + H(n^*)(n, B_2(\varphi)) + PB_4(n)B_4(\varphi)\\ &= (n, \hat{\mathbb{A}}\varphi),\end{aligned}$$

and

$$(\hat{\mathbb{A}}n, n) = \frac{3}{2\delta t}(n, n) - c(\Delta n, n) + H(n^*)(B_2(n), n) + P(B_4(n), n) \geq \frac{3}{2\delta t}\|n\|^2.$$

Therefore, the operator $\hat{\mathbb{A}}$ is symmetric positive definite. □

Let us define $\|n\|_{\hat{\mathbb{A}}} = \sqrt{(\hat{\mathbb{A}}n, n)}$ for any $n \in L^2_{per}(\Omega)$ and the subset $\mathbf{X} = \{n \in L^2_{per}(\Omega) : \|n\|_{\hat{\mathbb{A}}} < \infty\}$. Similarly as before, we can show that the linear system admits a unique weak solution in $\mathbf{X}$.

Theorem 3.4. *The second order linear system (3.29)-(3.31) is unconditionally energy stable, that is, it satisfies the following discrete energy dissipation law*

$$E_2^{k+1,k} \leq E_2^{k,k-1} - \delta t \left\| \frac{3n^{k+1} - 4n^k + n^{k-1}}{2\delta t} \right\|^2, \tag{3.32}$$

where

$$E_2^{k+1,k} = \frac{c}{4}\Big(\left\|\nabla n^{k+1}\right\|^2 + \left\|2\nabla n^{k+1} - \nabla n^k\right\|^2 \Big) + \frac{1}{2}\Big(\left\|W^{k+1}\right\|^2 + \left\|2W^{k+1} - W^k\right\|^2 \Big) + \frac{P}{4}((V^{k+1})^2 + (2V^{k+1} - V^k)^2).$$

Proof. By taking the L^2 inner product of (3.29) with $3n^{k+1} - 4n^k + n^{k-1}$, we have

$$\frac{1}{2\delta t}\left\|3n^{k+1} - 4n^k + n^{k-1}\right\|^2 = c(\Delta n^{k+1}, 3n^{k+1} - 4n^k + n^{k-1}) - (H(n^*)W^{k+1}, 3n^{k+1} - 4n^k + n^{k-1}) - P(V^{k+1}, 3n^{k+1} - 4n^k + n^{k-1}). \tag{3.33}$$

By taking the L^2 inner product of (3.30) with W^{k+1}, we obtain

$$(3W^{k+1} - 4W^k + W^{k-1}, W^{k+1}) = \frac{1}{2}H(n^*)(3n^{k+1} - 4n^k + n^{k-1}, W^{k+1}),$$

and by applying the following identity

$$2(3a - 4b + c, a) = |a|^2 - |b|^2 + |2a - b|^2 - |2b - c|^2 + |a - 2b + c|^2, \tag{3.34}$$

we obtain

$$\left\|W^{k+1}\right\|^2 - \left\|W^k\right\|^2 + \left\|2W^{k+1} - W^k\right\|^2 - \left\|2W^k - W^{k-1}\right\|^2 + \left\|W^{k+1} - 2W^k + W^{k-1}\right\|^2 = (H(n^*)W^{k+1}, 3n^{k+1} - 4n^k + n^{k-1}). \tag{3.35}$$

By taking the simple multiplication of (3.31) with PV^{k+1} and applying (3.34), we have

$$\frac{P}{2}((V^{k+1})^2 - (V^k)^2 + (2V^{k+1} - V^k)^2 - (2V^k - V^{k-1})^2 + (V^{k+1} - 2V^k + V^{k-1})^2) = P(V^{k+1}, 3n^{k+1} - 4n^k + n^{k-1}). \tag{3.36}$$

Combination of (3.33), (3.35) and (3.36) gives us

$$\begin{aligned}
&\frac{c}{2}\Big(\left\|\nabla n^{k+1}\right\|^2 - \left\|\nabla n^{k}\right\|^2 + \left\|2\nabla n^{k+1} - \nabla n^{k}\right\|^2 - \left\|2\nabla n^{k} - \nabla n^{k-1}\right\|^2 \\
&+ \left\|\nabla n^{k+1} - 2\nabla n^{k} + \nabla n^{k-1}\right\|^2 \Big) + \Big(\left\|W^{k+1}\right\|^2 - \left\|W^{k}\right\|^2 + \left\|2W^{k+1} - W^{k}\right\|^2 \\
&- \left\|2W^{k} - W^{k-1}\right\|^2 + \left\|W^{k+1} - 2W^{k} + W^{k-1}\right\|^2 \Big) + \frac{P}{2}((V^{k+1})^2 - (V^{k})^2 \\
&+(2V^{k+1} - V^{k})^2 - (2V^{k} - V^{k-1})^2 + (V^{k+1} - 2V^{k} + V^{k-1})^2) \\
&= -\frac{1}{2\delta t}\left\|3n^{k+1} - 4n^{k} + n^{k-1}\right\|^2,
\end{aligned}$$

i.e.,

$$\begin{aligned}
&\frac{c}{2}(\left\|\nabla n^{k+1}\right\|^2 + \left\|2\nabla n^{k+1} - \nabla n^{k}\right\|^2 + \left\|\nabla n^{k+1} - 2\nabla n^{k} + \nabla n^{k-1}\right\|^2) \\
&+ \left\|W^{k+1}\right\|^2 + \left\|2W^{k+1} - W^{k}\right\|^2 + \left\|W^{k+1} - 2W^{k} + W^{k-1}\right\|^2 \\
&+\frac{P}{2}((V^{k+1})^2 + (2V^{k+1} - V^{k})^2 + (V^{k+1} - 2V^{k} + V^{k-1})^2) \\
&= \frac{c}{2}(\left\|\nabla n^{k}\right\|^2 + \left\|2\nabla n^{k} - \nabla n^{k-1}\right\|^2) + \left\|W^{k}\right\|^2 + \left\|2W^{k} - W^{k-1}\right\|^2 \\
&+\frac{P}{2}((V^{k})^2 + (2V^{k} - V^{k-1})^2) - \frac{1}{2\delta t}\left\|3n^{k+1} - 4n^{k} + n^{k-1}\right\|^2. \qquad (3.37)
\end{aligned}$$

Finally, after dropping some positive terms from above equation (3.37), we have the discrete energy law (3.32). □

Chapter 4

Numerical schemes for multi-component system

In this chapter, we focus our study on a multi-component system with $M \geq 2$, that is, a system with a mixture of different substances. We will design first and second order numerical time stepping schemes to solve the diffuse interface model problem with Peng-Robinson equation of state for this system.

4.1 Multi-component system

As a result, we then have a highly coupled gradient contribution for the inhomogeneous term

$$f_{\nabla}(\mathbf{n}; T) = \frac{1}{2} \sum_{i,j=1}^{M} c_{ij} \nabla n_i \cdot \nabla n_j.$$

Some efforts must be taken in order to decouple the relations between different components. Therefore, we introduce the following linear transformation to simplify the system.

4.1.1 Transformed system

Recall the crossed influence parameters c_{ij} in the diffuse interface model, they are generally described as the modified geometric mean of the pure component influence parameters c_i and c_j by

$$c_{ij} = (1 - \beta_{ij}) \sqrt{c_i c_j}, \tag{4.1}$$

where the parameters β_{ij} are binary interaction coefficients for the influence parameters. The influence parameter matrix is denoted by $\mathbf{C} = (c_{ij})_{i,j=1}^{M}$.

In this work, suitable parameters β_{ij} are chosen such that $\mathbf{C}$ is symmetric positive definite. Therefore there exists $\mathbf{Q}^T\mathbf{Q} = \mathbf{Q}\mathbf{Q}^T = I$ such that $\mathbf{C} = \mathbf{Q}\Lambda\mathbf{Q}^T$, where $\Lambda = \text{diag}(\lambda_1, \cdots, \lambda_M)$ and λ_i $(i = 1, 2, \cdots, M)$ denote the real positive eigenvalues of $\mathbf{C}$. We next define an orthonormal transformation matrix $\mathbf{Q} = [\mathbf{q}_1, \cdots, \mathbf{q}_M]$ where $\mathbf{q}_i$ $(i = 1, 2, \cdots, M)$ are orthonormal eigenvectors corresponding to eigenvalues λ_i $(i = 1, 2, \cdots, M)$. Applying this orthonormal transformation, we define a vector $\mathbf{\Phi} = [\phi_1, \cdots, \phi_M]^T$ as

$$\mathbf{\Phi} = \mathbf{Q}^T\mathbf{n}, \quad \mathbf{n} = \mathbf{Q}\mathbf{\Phi}. \tag{4.2}$$

Denote $g(\mathbf{\Phi}) = f_0(\mathbf{n}) = f_0(\mathbf{Q}\mathbf{\Phi})$. Using the relations given by (4.2), we have

$$\sum_{i,j=1}^{M} c_{ij}\nabla n_i \cdot \nabla n_j = \sum_{i=1}^{M} \lambda_i |\nabla \phi_i|^2. \tag{4.3}$$

As a result, the highly coupled linear term are simplified and we have an equivalent free energy in term of the new variables introduced, which can be represented as

$$E(\phi) = \int_\Omega \Big(\frac{1}{2} \sum_{i=1}^{M} \lambda_i |\nabla \phi_i|^2 + g(\phi)) \Big) d\mathbf{x}. \tag{4.4}$$

4.1.2 Invariant energy quadratization and stablization

Based on the variational approach, we have

$$\frac{\partial \phi_i}{\partial t} = -\frac{\delta E(\phi)}{\delta \phi_i} = \lambda_i \Delta \phi_i - \frac{\partial g(\phi)}{\partial \phi_i}, \quad i = 1, 2, \cdots, M, \tag{4.5}$$

which is equivalent to

$$\frac{\partial \phi_i}{\partial t} = (\lambda_i \Delta \phi_i - \kappa \phi_i) - \left(\frac{\delta g(\phi)}{\delta \phi_i} - \kappa \phi_i \right), \tag{4.6}$$

after introducing stabilizer κ_i which satisfies $\kappa_i \geq \frac{1}{2}\max\{0, \max_{\phi} \frac{\partial^2 g(\phi)}{\partial \phi_i^2}\}$ for each i.

Correspondingly, the free energy (4.4) can be rewritten as

$$E(\phi) = \int_\Omega \left\{ \frac{1}{2} \sum_{i=1}^{M} (\lambda_i |\nabla \phi_i|^2 + \kappa_i \phi_i^2) + \tilde{g}(\phi) \right\} d\mathbf{x}, \tag{4.7}$$

where $\tilde{g}(\phi) = g(\phi) - \frac{1}{2}\sum\limits_{i=1}^{M}\kappa_i\phi_i^2$.

Assuming that function $\tilde{g}(\phi)$ is bounded from below, that is, $\tilde{g}(\phi) \geq -B_0$ for some constant $B_0 \geq 0$. The free energy can be reformed as

$$E(\phi) = \int_\Omega \left\{ \frac{1}{2}\sum_{i=1}^{M}(\lambda_i|\nabla\phi_i|^2 + \kappa_i\phi_i^2) + \left(\sqrt{\tilde{g}(\phi) + B_0}\right)^2 - B_0 \right\} d\mathbf{x}. \tag{4.8}$$

Since we only add a zero term therein, we emphasize that the free energy is invariant.

By introducing the auxiliary variables $W = \sqrt{\tilde{g}(\phi) + B_0}$ and $\psi_i = \int_\Omega \phi_i d\mathbf{x} - \tilde{N}_i$ ($i = 1, 2, \cdots, M$), the modified free energy functional can be expressed as the following

$$E(\phi, W, \psi) = \int_\Omega \left\{ \frac{1}{2}\sum_{i=1}^{M}(\lambda_i|\nabla\phi_i|^2 + \kappa_i\phi_i^2) + W^2 - B_0 \right\} d\mathbf{x} + \frac{1}{2}\sum_{i=1}^{M} P_i\psi_i^2, \tag{4.9}$$

where $\tilde{N}_i = \mathbf{q}_i^T\mathbf{N}$ and P_i are penalty parameters to retain mass constraint for all components.

4.1.3 Energy dissipation law

Based on the variational approach, we have

$$\frac{\partial\phi_i}{\partial t} = -\frac{\delta E(\phi, W, \psi)}{\delta\phi_i} = \lambda_i\Delta\phi_i - \kappa_i\phi_i - W(\phi)H(\phi_i) - P_i\psi_i, \tag{4.10}$$

where $H(\phi_i) = \frac{\frac{\partial\tilde{g}(\phi)}{\partial\phi_i} - \kappa_i\phi_i}{\sqrt{\tilde{g}(\phi)+B_0}}$. Then, we obtain a new, but equivalent partial differential system as follows:

$$\begin{cases} \dfrac{\partial\phi_i}{\partial t} = \lambda_i\Delta\phi_i - \kappa_i\phi_i - W(\phi)H(\phi_i) - P_i\psi_i, & (4.11) \\ \dfrac{\partial W}{\partial t} = \dfrac{1}{2}\displaystyle\sum_{i=1}^{M} H(\phi_i)\frac{\partial\phi_i}{\partial t}, & (4.12) \\ \dfrac{\partial\psi_i}{\partial t} = \displaystyle\int_\Omega \frac{\partial\phi_i}{\partial t} d\mathbf{x}, & (4.13) \end{cases}$$

with the initial conditions

$$\phi_i|_{(t=0)} = \phi_{i0}, \quad W|_{(t=0)} = \sqrt{\tilde{g}(\phi_{i0}) + B_0}, \quad \psi_i|_{(t=0)} = 0, \tag{4.14}$$

for $i = 1, 2, \cdots, M$.

Taking the L^2-inner product of (4.11) with $\frac{\partial \phi_i}{\partial t}$, of (4.12) with W, and taking the simple multiplication of (4.13) with $P_i\psi_i$, summing them up, we then get the energy dissipation law of the modified system (4.11)-(4.13) as follows

$$\frac{d}{dt}E(\phi, W, \psi) = -\sum_{i=1}^{M}\left\|\frac{\partial \phi_i}{\partial t}\right\|^2 \leq 0. \tag{4.15}$$

4.2 Numerical schemes for time integration

In this section, we present linear time stepping schemes of first and second order to solve the system (4.11)-(4.13).

4.2.1 First order scheme

Assuming that ϕ_i^k, W^k and ψ_i^k are already known, then we solve ϕ_i^{k+1}, W^{k+1} and ψ_i^{k+1} from the following first order temporal semi-discretized system

$$\begin{cases} \dfrac{\phi_i^{k+1}-\phi_i^k}{\delta t} = \lambda_i \Delta \phi_i^{k+1} - \kappa_i \phi_i - W^{k+1} H(\phi_i^k) - P_i \psi_i^{k+1}, & (4.16) \\ \dfrac{W^{k+1}-W^k}{\delta t} = \dfrac{1}{2}\displaystyle\sum_{i=1}^{M} H(\phi_i^k)\frac{\phi_i^{k+1}-\phi_i^k}{\delta t}, & (4.17) \\ \dfrac{\psi_i^{k+1}-\psi_i^k}{\delta t} = \displaystyle\int_\Omega \frac{\phi_i^{k+1}-\phi_i^k}{\delta t} d\mathbf{x}, & (4.18) \end{cases}$$

where $1 \leq i \leq M$.

From (4.17) and (4.18), we have

$$\begin{aligned} W^{k+1} &= W^k - \frac{1}{2}\sum_{i=1}^{M} H(\phi_i^k)\phi_i^k + \frac{1}{2}\sum_{i=1}^{M} H(\phi_i^k)\phi_i^{k+1} \triangleq A_{W1} + A_{W2}(\phi_i^{k+1}), \\ \psi_i^{k+1} &= \psi_i^k - \int_\Omega \phi_i^k d\mathbf{x} + \int_\Omega \phi_i^{k+1} d\mathbf{x} \triangleq A_{3i} + A_{4i}(\phi_i^{k+1}). \end{aligned}$$

Then the system (4.16)-(4.18) can be rewritten as

$$\begin{aligned} &\frac{\phi_i^{k+1}}{\delta t} - \lambda_i \Delta \phi_i^{k+1} + \kappa_i \phi_i^{k+1} + H(\phi_i^k) A_{W2}(\phi_i^{k+1}) + P_i A_{4i}(\phi_i^{k+1}) \\ &\qquad = \frac{\phi_i^k}{\delta t} - H(\phi_i^k) A_{W1} - P_i A_{3i}, \quad 1 \leq i \leq M. \end{aligned} \tag{4.19}$$

The above linear system can be denoted as $\mathbb{A}\phi = \mathbf{b}$.

Theorem 4.1. *The linear operator $\mathbb{A}$ is symmetric positive definite.*

Proof. Assuming $\rho = [\rho_1, \rho_2, \cdots, \rho_M]^T$, we have

$$\begin{aligned}
(\mathbb{A}\phi, \rho) &= \frac{1}{\delta t}\sum_{i=1}^{M}(\phi_i, \rho_i) - \sum_{i=1}^{M}\lambda_i(\Delta\phi_i, \rho_i) + \sum_{i=1}^{M}\kappa_i(\phi_i, \rho_i) + \sum_{i=1}^{M}H(\phi_i^k)(A_{W2}(\phi_i), \rho_i) \\
&\quad + \sum_{i=1}^{M}P_i(A_{4i}(\phi_i), \rho_i) \\
&= + \frac{1}{\delta t}\sum_{i=1}^{M}(\phi_i, \rho_i) - \sum_{i=1}^{M}\lambda_i(\phi_i, \Delta\rho_i) + \sum_{i=1}^{M}\kappa_i(\rho_i, \phi_i) + \sum_{i=1}^{M}H(\phi_i^k)(A_{W2}(\rho_i), \phi_i) \\
&\quad + \sum_{i=1}^{M}P_iA_{4i}(\phi_i)A_{4i}(\rho_i) \\
&= (\mathbb{A}\rho, \phi),
\end{aligned}$$

and

$$\begin{aligned}
(\mathbb{A}\phi, \phi) &= \frac{1}{\delta t}\sum_{i=1}^{M}(\phi_i, \phi_i) - \sum_{i=1}^{M}\lambda_i(\Delta\phi_i, \phi_i) + \sum_{i=1}^{M}\kappa_i(\phi_i, \phi_i) + \sum_{i=1}^{M}H(\phi_i^k)(A_{W2}(\phi_i), \phi_i) \\
&\quad + \sum_{i=1}^{M}P_i(A_{4i}(\phi_i), \phi_i) \\
&= \frac{1}{\delta t}\sum_{i=1}^{M}(\phi_i, \phi_i) + \sum_{i=1}^{M}\lambda_i(\nabla\phi_i, \nabla\phi_i) + \sum_{i=1}^{M}\kappa_i(\phi_i, \phi_i) \\
&\quad + \frac{1}{2}\left(\sum_{i=1}^{M}H(\phi_i^k)\phi_i, \sum_{i=1}^{M}H(\phi_i^k)\phi_i\right) + \sum_{i=1}^{M}P_iA_{4i}(\phi_i)A_{4i}(\phi_i) \\
&\geq \frac{1}{\delta t}\sum_{i=1}^{M}\|\phi_i\|^2.
\end{aligned}$$

Therefore, the operator $\mathbb{A}$ is symmetric positive definite. □

Let us define the norm $\|\phi\|_{\mathbb{A}} = \sqrt{(\mathbb{A}\phi, \phi)}$ for any $\phi \in L^2_{per}(\Omega)$ and the subset $\mathbf{X} = \{\phi \in L^2_{per}(\Omega) : \|\phi\|_{\mathbb{A}} < \infty\}$, where $L^2_{per}(\Omega)$ denotes the subspace of all functions $\phi \in L^2(\Omega)$ with periodic or no-flux boundary conditions.

It is easy to show that $\|\phi\|_{\mathbb{A}}$ is a norm for $L^2_{per}(\Omega)$ and $\mathbf{X}$ is a Hilbert subspace associated with the norm $\|\phi\|_{\mathbb{A}}$. The well-posedness of the linear system $\mathbb{A}\phi = \mathbf{b}$ in the weak sense comes from the Lax-Milgram theorem, i.e., the linear system (4.19) admits a unique weak solution in $\mathbf{X}$.

Theorem 4.2. *The first order linear scheme (4.16)-(4.18) is unconditionally energy stable, i.e., satisfies the following discrete energy dissipation law*

$$E_{1st}^{k+1} \leq E_{1st}^{k} - \frac{1}{\delta t}\sum_{i=1}^{M}\|\phi_i^{k+1} - \phi_i^k\|^2, \tag{4.20}$$

where

$$E_{1st}^{k} = \frac{1}{2}\sum_{i=1}^{M}\Big(\lambda_i\|\nabla\phi_i^k\|^2 + \kappa_i\|\phi_i^k\|^2 + P_i(\psi_i^k)^2\Big) + ||W^k||^2. \tag{4.21}$$

Proof. By taking the L^2 inner product of (4.16) with $\phi_i^{k+1} - \phi_i^k$, and summing from $i = 1$ to M, we have

$$\begin{aligned}\frac{1}{\delta t}\sum_{i=1}^{M}\|\phi_i^{k+1} - \phi_i^k\|^2 &= \sum_{i=1}^{M}\lambda_i\Big(\Delta\phi_i^{k+1}, \phi_i^{k+1} - \phi_i^k\Big) - \sum_{i=1}^{M}\kappa_i\Big(\phi_i^{k+1}, \phi_i^{k+1} - \phi_i^k\Big)\\ &- \sum_{i=1}^{M}\Big(W^{k+1}H(\phi_i^k), \phi_i^{k+1} - \phi_i^k\Big) - \sum_{i=1}^{M}P_i\Big(\psi_i^{k+1}, \phi_i^{k+1} - \phi_i^k\Big).\end{aligned} \tag{4.22}$$

By taking the L^2 inner product of (4.17) with W^{k+1}, we have

$$2\Big(W^{k+1} - W^k, W^{k+1}\Big) = \sum_{i=1}^{M}\Big(W^{k+1}H(\phi_i^k), \phi_i^{k+1} - \phi_i^k\Big). \tag{4.23}$$

By taking the simple multiplication of (4.18) with $P_i\psi_i^{k+1}$, and summing from $i = 1$ to M, we obtain

$$\sum_{i=1}^{M}P_i\Big(\psi_i^{k+1} - \psi_i^k\Big)\psi_i^{k+1} = \sum_{i=1}^{M}P_i\Big(\psi_i^{k+1}, \phi_i^{k+1} - \phi_i^k\Big). \tag{4.24}$$

Combining (4.22)-(4.24), and applying the identity (3.25) we obtain

$$\begin{aligned}&\frac{1}{2}\sum_{i=1}^{M}\lambda_i\|\nabla\phi_i^{k+1}\|^2 + \|W^{k+1}\|^2 + \frac{1}{2}\sum_{i=1}^{M}P_i(\psi_i^{k+1})^2 + \frac{1}{2}\sum_{i=1}^{M}\lambda_i\|\nabla\phi_i^{k+1} - \nabla\phi_i^k\|^2\\ &+\|W^{k+1} - W^k\|^2 + \frac{1}{2}\sum_{i=1}^{M}P_i(\psi_i^{k+1} - \psi_i^k)^2 + \frac{1}{2}\sum_{i=1}^{M}\kappa\|\phi_i^{k+1}\|^2 + \frac{1}{2}\sum_{i=1}^{M}\kappa\|\phi_i^{k+1} - \phi_i^k\|^2\\ &= \frac{1}{2}\sum_{i=1}^{M}\lambda_i\|\nabla\phi_i^k\|^2 + \|W^k\|^2 + \frac{1}{2}\sum_{i=1}^{M}P_i(\psi_i^k)^2 + \frac{1}{2}\sum_{i=1}^{M}\kappa\|\phi_i^k\|^2 - \frac{1}{\delta t}\sum_{i=1}^{M}\|\phi_i^{k+1} - \phi_i^k\|^2.\end{aligned}$$

Finally, we obtain result (4.20) after dropping some positive terms from last equation.

□

4.2.2 Second order scheme

The second order time stepping scheme to solve the system (4.11)-(4.13) is developed based on the second order backward differentiation formulas (BDF2). Assuming that ϕ_i^{k-1}, W^{k-1}, ψ_i^{k-1}, and ϕ_i^k, W^k, ψ_i^k are already known, then we solve ϕ_i^{k+1}, W^{k+1} and ψ_i^{k+1} from following second order temporal semi-discretized system

$$\begin{cases} \dfrac{3\phi_i^{k+1}-4\phi_i^k+\phi_i^{k-1}}{2\delta t} = \lambda_i\Delta\phi_i^{k+1} - \kappa_i\phi_i^{k+1} - W^{k+1}H(\phi_i^*) - P_i\psi_i^{k+1}, & (4.25) \\ \dfrac{3W^{k+1}-4W^k+W^{k-1}}{2\delta t} = \dfrac{1}{2}\displaystyle\sum_{i=1}^{M} H(\phi_i^*)\dfrac{3\phi_i^{k+1}-4\phi_i^k+\phi_i^{k-1}}{2\delta t}, & (4.26) \\ \dfrac{3\psi_i^{k+1}-4\psi_i^k+\psi_i^{k-1}}{2\delta t} = \displaystyle\int_\Omega \dfrac{3\phi_i^{k+1}-4\phi_i^k+\phi_i^{k-1}}{2\delta t}d\mathbf{x}, & (4.27) \end{cases}$$

where $\phi_i^* = 2\phi_i^k - \phi_i^{k-1}$.

For (4.26) and (4.27), we have

$$\begin{aligned} W^{k+1} &= \frac{4W^k - W^{k-1}}{3} - \frac{1}{2}\sum_{i=1}^{M} H(\phi_i^*)\frac{4\phi_i^k-\phi_i^{k-1}}{3} + \frac{1}{2}\sum_{i=1}^{M} H(\phi_i^*)\phi_i^{k+1}, \\ \psi_i^{k+1} &= \frac{4\psi_i^k - \psi_i^{k-1}}{3} - \int_\Omega \frac{4\phi_i^k-\phi_i^{k-1}}{3}d\mathbf{x} + \int_\Omega \phi_i^{k+1}d\mathbf{x}. \end{aligned}$$

Set

$$\begin{aligned} B_1 &= W^+ - \frac{1}{2}\sum_{i=1}^{M} H(\phi_i^*)\phi_i^+, \quad B_2(\phi) = \frac{1}{2}\sum_{i=1}^{M} H(\phi_i^*)\phi_i, \\ B_{3i} &= \psi_i^+ - \int_\Omega \phi_i^+ d\mathbf{x}, \qquad B_{4i}(\phi_i) = \int_\Omega \phi_i d\mathbf{x}, \end{aligned}$$

where $S^+ = \frac{4S^k - S^{k-1}}{3}$.

We have the following reduced linear system

$$\begin{aligned} &\frac{3}{2\delta t}\phi_i^{k+1} - \lambda_i\Delta\phi_i^{k+1} + \kappa_i\phi_i^{k+1} + H(\phi_i^*)B_2(\phi^{k+1}) + PB_{4i}(\phi_i^{k+1}) \\ &\quad = \frac{1}{2\delta t}(4\phi_i^k - \phi_i^{k-1}) - H(\phi_i^*)B_1 - PB_{3i}, \quad 1 \le i \le M. \end{aligned} \tag{4.28}$$

The above linear system can be expressed as $\hat{\mathbb{A}}\phi^{k+1} = \hat{\mathbf{b}}$, and we need solve for ϕ^{k+1} from it.

Theorem 4.3. *The linear operator $\hat{\mathbb{A}}$ is symmetric positive definite.*

Proof. Assuming $\rho = [\rho_1, \rho_2, \cdots, \rho_M]^T$, we have

$$\begin{aligned}
(\hat{\mathbb{A}}\phi, \rho) &= \frac{3}{2\delta t}\sum_{i=1}^{M}(\phi_i, \rho_i) - \sum_{i=1}^{M}\lambda_i(\Delta\phi_i, \rho_i) + \sum_{i=1}^{M}\kappa_i(\phi_i, \rho_i) + \sum_{i=1}^{M}H(\phi_i^*)(B_2(\phi_i), \rho_i) \\
&\quad + \sum_{i=1}^{M}P_i(B_{4i}(\phi_i), \rho_i) \\
&= \frac{3}{2\delta t}\sum_{i=1}^{M}(\phi_i, \rho_i) - \sum_{i=1}^{M}\lambda_i(\phi_i, \Delta\rho_i) + \sum_{i=1}^{M}\kappa_i(\rho_i, \phi_i) + \sum_{i=1}^{M}H(\phi_i^*)(B_2(\rho_i), \phi_i) \\
&\quad + \sum_{i=1}^{M}P_iB_{4i}(\phi_i)B_{4i}(\rho_i) \\
&= (\hat{\mathbb{A}}\rho, \phi),
\end{aligned}$$

and

$$\begin{aligned}
(\hat{\mathbb{A}}\phi, \phi) &= \frac{3}{2\delta t}\sum_{i=1}^{M}(\phi_i, \phi_i) - \sum_{i=1}^{M}\lambda_i(\Delta\phi_i, \phi_i) + \sum_{i=1}^{M}\kappa_i(\phi_i, \phi_i) \\
&\quad + \sum_{i=1}^{M}H(\phi_i^*)(B_2(\phi_i), \phi_i) + \sum_{i=1}^{M}P_i(B_{4i}(\phi_i), \phi_i) \\
&= \frac{3}{2\delta t}\sum_{i=1}^{M}(\phi_i, \phi_i) + \sum_{i=1}^{M}\lambda_i(\nabla\phi_i, \nabla\phi_i) + \sum_{i=1}^{M}\kappa_i(\phi_i, \phi_i) \\
&\quad + \frac{1}{2}\left(\sum_{i=1}^{M}H(\phi_i^*)\phi_i, \sum_{i=1}^{M}H(\phi_i^*)\phi_i\right) + \sum_{i=1}^{M}P_iB_{4i}(\phi_i)B_{4i}(\phi_i) \\
&\geq \frac{3}{2\delta t}\sum_{i=1}^{M}\|\phi_i\|^2.
\end{aligned}$$

Therefore, the operator $\hat{\mathbb{A}}$ is symmetric positive definite. □

Define $\|\phi\|_{\hat{\mathbb{A}}} = \sqrt{(\hat{\mathbb{A}}\phi, \phi)}$ for any $\phi \in L^2_{per}(\Omega)$ and the subset $\mathbf{X} = \{\phi \in L^2_{per}(\Omega) : \|\phi\|_{\hat{\mathbb{A}}} < \infty\}$, where $L^2_{per}(\Omega)$ denotes the subspace of all functions $\phi \in L^2(\Omega)$ with periodic or no-flux boundary condition. It is easy to show that $\|\phi\|_{\hat{\mathbb{A}}}$ is a norm for $L^2_{per}(\Omega)$ and $\mathbf{X}$ is a Hilbert subspace associated with the norm $\|\phi\|_{\hat{\mathbb{A}}}$. The well-posedness of the linear system $\hat{\mathbb{A}}\phi = \hat{b}$ in the weak sense comes from the Lax-Milgram theorem, i.e., the linear system (4.28) admits a unique weak solution in $\mathbf{X}$.

Theorem 4.4. *The second order linear system (4.25)-(4.27) is unconditionally energy stable, that is, satisfies the following discrete energy dissipation law*

$$E_{BDF2}^{k+1,k} \leq E_{BDF2}^{k,k-1} - \delta t \sum_{i=1}^{M} \| \frac{3\phi_i^{k+1} - 4\phi_i^k + \phi_i^{k-1}}{2\delta t} \|^2, \tag{4.29}$$

where

$$\begin{aligned} E_{BDF2}^{k+1,k} = & \frac{1}{4} \sum_{i=1}^{M} (\lambda_i (\|\nabla \phi_i^{k+1}\|^2 + \|2\nabla \phi_i^{k+1} - \nabla \phi_i^k\|^2) + \kappa_i (\|\phi_i^{k+1}\|^2 + \|2\phi_i^{k+1} - \phi_i^k\|^2) \\ & + P_i((\psi_i^{k+1})^2 + (2\psi_i^{k+1} - \psi_i^k)^2)) + \frac{1}{2}(\|W^{k+1}\|^2 + \|2W^{k+1} - W^k\|^2). \end{aligned}$$

Proof. By taking the L^2 inner product of (4.25) with $3\phi_i^{k+1} - 4\phi_i^k + \phi_i^{k-1}$, and summing from $i = 1$ to M, we have

$$\begin{aligned} \frac{1}{2\delta t} \sum_{i=1}^{M} \|3\phi_i^{k+1} - 4\phi_i^k + \phi_i^{k-1}\|^2 = & \sum_{i=1}^{M} \Big[\lambda_i \left(\Delta \phi_i^{k+1}, 3\phi_i^{k+1} - 4\phi_i^k + \phi_i^{k-1} \right) \\ & - \kappa_i \left(\phi_i^{k+1}, 3\phi_i^{k+1} - 4\phi_i^k + \phi_i^{k-1} \right) \\ & - \left(H(\phi_i^*) W^{k+1}, 3\phi_i^{k+1} - 4\phi_i^k + \phi_i^{k-1} \right) \\ & - P_i \left(\psi_i^{k+1}, 3\phi_i^{k+1} - 4\phi_i^k + \phi_i^{k-1} \right) \Big]. \end{aligned} \tag{4.30}$$

By taking the L^2 inner product of (4.26) with W^{k+1}, we obtain

$$(3W^{k+1} - 4W^k + W^{k-1}, W^{k+1}) = \frac{1}{2} \sum_{i=1}^{M} H(\phi_i^*)(3\phi_i^{k+1} - 4\phi_i^k + \phi_i^{k-1}, W^{k+1}). \tag{4.31}$$

By taking the L^2 inner product of (4.27) with $P_i \psi_i^{k+1}$, and summing from $i = 1$ to M, we get

$$\sum_{i=1}^{M} P_i (3\psi_i^{k+1} - 4\psi_i^k + \psi_i^{k-1}) \psi_i^{k+1} = \sum_{i=1}^{M} P_i (\psi_i^{k+1}, 3\phi_i^{k+1} - 4\phi_i^k + \phi_i^{k-1}). \tag{4.32}$$

Combining (4.30)-(4.32), and applying the identity (3.34) we have

$$\begin{aligned}
&\frac{1}{2}\sum_{i=1}^{M}\Big[\lambda_i\Big(\|\nabla\phi_i^{k+1}\|^2-\|\nabla\phi_i^{k}\|^2+\|2\nabla\phi_i^{k+1}-\nabla\phi_i^{k}\|^2-\|2\nabla\phi_i^{k}-\nabla\phi_i^{k-1}\|^2\\
&\quad+\|\nabla\phi_i^{k+1}-2\nabla\phi_i^{k}+\nabla\phi_i^{k-1}\|^2\Big)+\kappa_i\Big(\|\phi_i^{k+1}\|^2-\|\phi_i^{k}\|^2+\|2\phi_i^{k+1}-\phi_i^{k}\|^2\\
&\quad-\|2\phi_i^{k}-\phi_i^{k-1}\|^2+\|\phi_i^{k+1}-2\phi_i^{k}+\phi_i^{k-1}\|^2\Big)+P_i((\psi_i^{k+1})^2-(\psi_i^{k})^2\\
&\quad+(2\psi_i^{k+1}-\psi_i^{k})^2-(2\psi_i^{k}-\psi_i^{k-1})^2+(\psi_i^{k+1}-2\psi_i^{k}+\psi_i^{k-1})^2\Big)\Big]+\|W^{k+1}\|^2\\
&\quad-\|W^{k}\|^2+\|2W^{k+1}-W^{k}\|^2-\|2W^{k}-W^{k-1}\|^2+\|W^{k+1}-2W^{k}+W^{k-1}\|^2\\
&=-\frac{1}{2\delta t}\sum_{i=1}^{M}\|3\phi_i^{k+1}-4\phi_i^{k}+\phi_i^{k-1}\|^2. \qquad (4.33)
\end{aligned}$$

Finally, dropping some positive terms from (4.33), we obtain the result (4.29). □

Chapter 5

Numerical experiments

In this chapter we present numerical experiments results for the diffuse interface model for both single and multiple components gas-liquid systems. For single-component system with $M = 1$ in the first part, we consider a pure substance fluid of isobutane (C_4H_{10}). For multi-component system in the second part, a mixture of isobutane (C_4H_{10}) and decane ($C_{10}H_{22}$) is used for the case $M = 2$. The critical properties used to calculate parameters in the models are listed in Table 5.1. All experiments are carried in the domain $\Omega = (0, L)^d$ with $L =$ 2.0E-08 meters and $d = 2, 3$ denotes the space dimension. The first order and second order invariant energy quadratization methods are denoted by IEQ-1 and IEQ-BDF2, respectively.

Table 5.1 Critical properties and parameters.

Symbol	$T_c(K)$	P_c	ω	m
C_4H_{10}	425.2	3.80 MPa	0.199	0.6708
$C_{10}H_{22}$	617.7	2.10 MPa	0.484	1.0578

5.1 Single-component system

5.1.1 Temporal accuracy test for single-component system

We first present numerical experiments in two dimensions to demonstrate the temporal accuracy of the two numerical schemes for the single-component system. For the initial configuration, we use the case of single droplet – the liquid density of isobutane under a saturated pressure condition at the temperature 350K is imposed in the

square subregion of $\left(\frac{3L}{8}, \frac{3L}{4}\right)^2$, and the rest of the domain is filled with a saturated gas of isobutane under the same temperature. In other words, about 14% of the total volume is saturated liquid, while the rest 86% is saturated gas.

We perform the refinement test of the time step size (Δt = 2.0E-2, 1.0E-2, $\cdots$, 1.5625E-4) for both the IEQ-1 and IEQ-BDF2 schemes, and choose the approximate solution obtained by applying the schemes with the small time step size Δt = 1.0E-6 as the benchmark solution for computing errors. The penalty parameter is set to be P = 1.0E+20. The spatial discretization is carried out using the central finite difference on the uniform 1024×1024 mesh of the domain Ω to remove the effect caused by the errors of spatial discretization. Define the L_2 relative error of the approximate solution for the molar density n by

$$L_2 = \frac{||n_* - n_h||}{||n_*||},$$

where n_* denotes the benchmark solution and n_h the numerical solution. Table 5.2 lists the L_2 relative errors and convergence rates of the numerical solutions at $t = 0.5$ with different time step sizes. It is easy to see that both the IEQ-1 and IEQ-BDF2 schemes work very stably for all time step sizes and show almost perfect first and second order accuracies. In addition, IEQ-BDF2 gives much better accuracy than IEQ-1 along the time step size refinement.

There is a large gradient contribution to the total Helmholtz free energy due to the jump in molar density between the gas and liquid regions. We will numerically simulate the time evolution of the molar density distribution and track the gas-liquid interface under the gradient flow in two and three dimensional spaces.

5.1.2 2D simulation

We perform experiments in 2D with different initial configurations. We use the IEQ-BDF2 scheme with Δt = 5.0E-3 and a uniform mesh of 512×512 and set the penalty parameter P = 1.0E+20.

Table 5.2 Convergence tests for single component system.

Time Step Size Δt	IEQ-1		IEQ-BDF2	
	Error	Conv. Rate	Error	Conv. Rate
2.0E-2	9.4836E-3	-	5.2778E-3	-
1.0E-2	4.6670E-3	1.023	1.8632E-3	1.503
5.0E-3	2.2616E-3	1.045	5.8986E-4	1.659
2.5E-3	1.1027E-3	1.036	1.6892E-4	1.804
1.25E-3	5.4286E-4	1.022	4.4680E-5	1.919
6.25E-4	2.6915E-4	1.012	1.1272E-5	1.987
3.125E-4	1.3401E-5	1.006	2.7880E-6	2.015
1.5625E-4	6.6855E-5	1.003	7.0398E-7	1.986

ONE DROPLET

Figure 5.1 presents the simulated molar density distribution for the one droplet case at different times ($t = 0, 1, 3, 5, 10, 20$, respectively) during the evolution. The initial configuration is the same as we used in the accuracy test. We can see that the shape of the droplet for the liquid is initially square, but its four corners are slowly rounded as the time increases, and finally appears to be a perfect circle. At the time $t = 20$ the steady state seems to be reached. As suggested in [40], the surface tension contribution of Helmholtz free energy density, f_{ST}, is defined by

$$f_{\mathrm{ST}} = 2f_{\nabla}(n) = c\nabla n \cdot \nabla n, \tag{5.1}$$

which can be used to better characterize the gas-liquid interface. The plots of the simulated surface tension contribution of Helmholtz free energy density at the same times are shown in Figure 5.2, and we can clearly see the movement of the interface along with the time. The corresponding plots of evolution of the total energy (3.4) and the mass are given in Figure 5.3. We observe that the energy decreases monotonically and the mass is accurately maintained with respect to the time. The energy decay is very fast initially then slows down as the solution approaches its steady state.

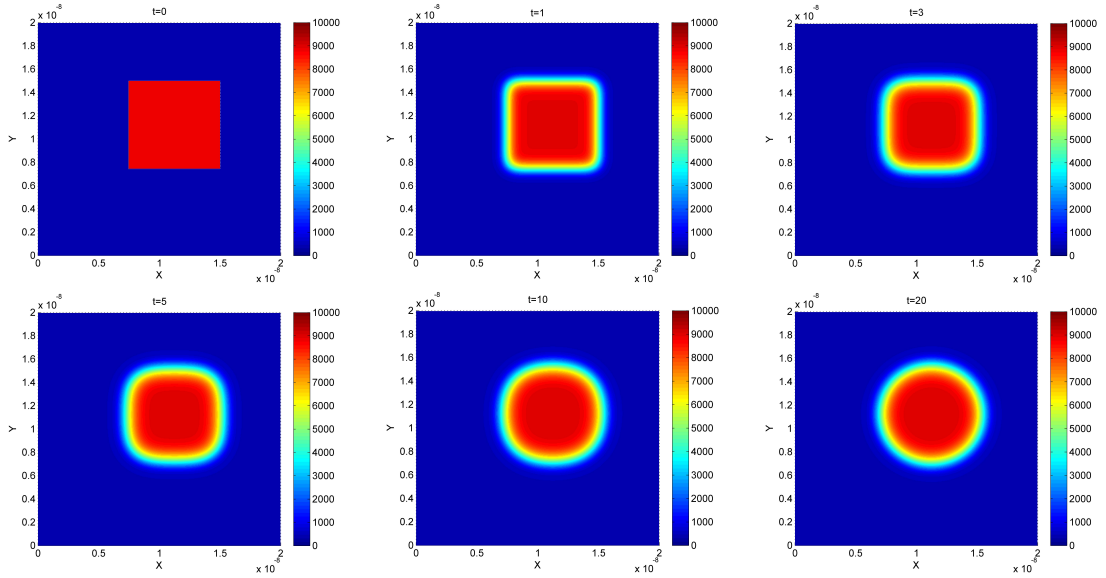

Figure 5.1 Dynamical evolution of one droplet in 2D: molar density distribution of C_4H_{10}.

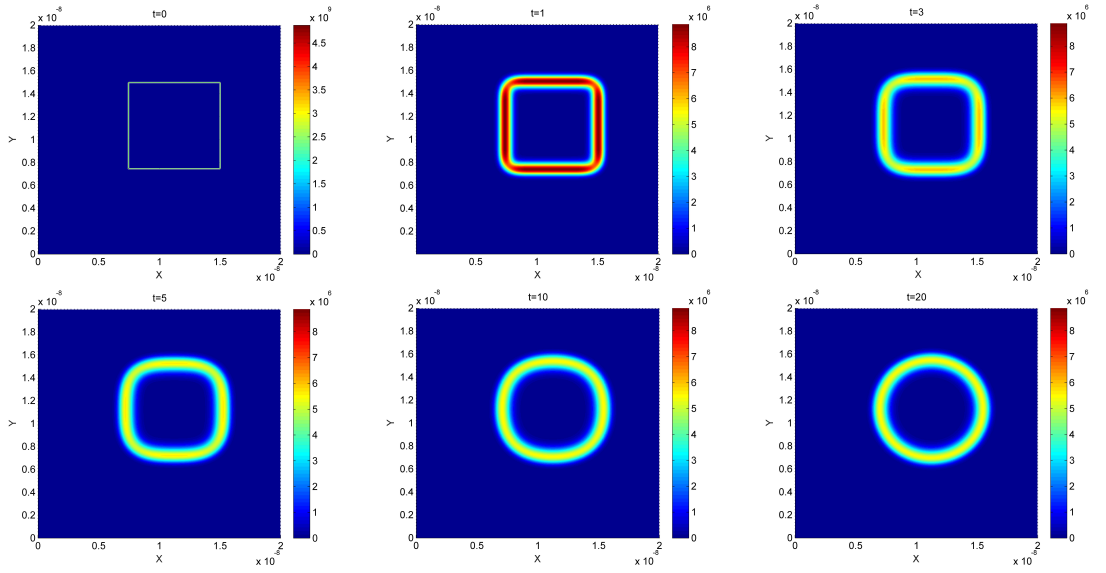

Figure 5.2 Dynamical evolution of one droplet in 2D: surface tension contribution of Helmholtz free energy density of C_4H_{10}.

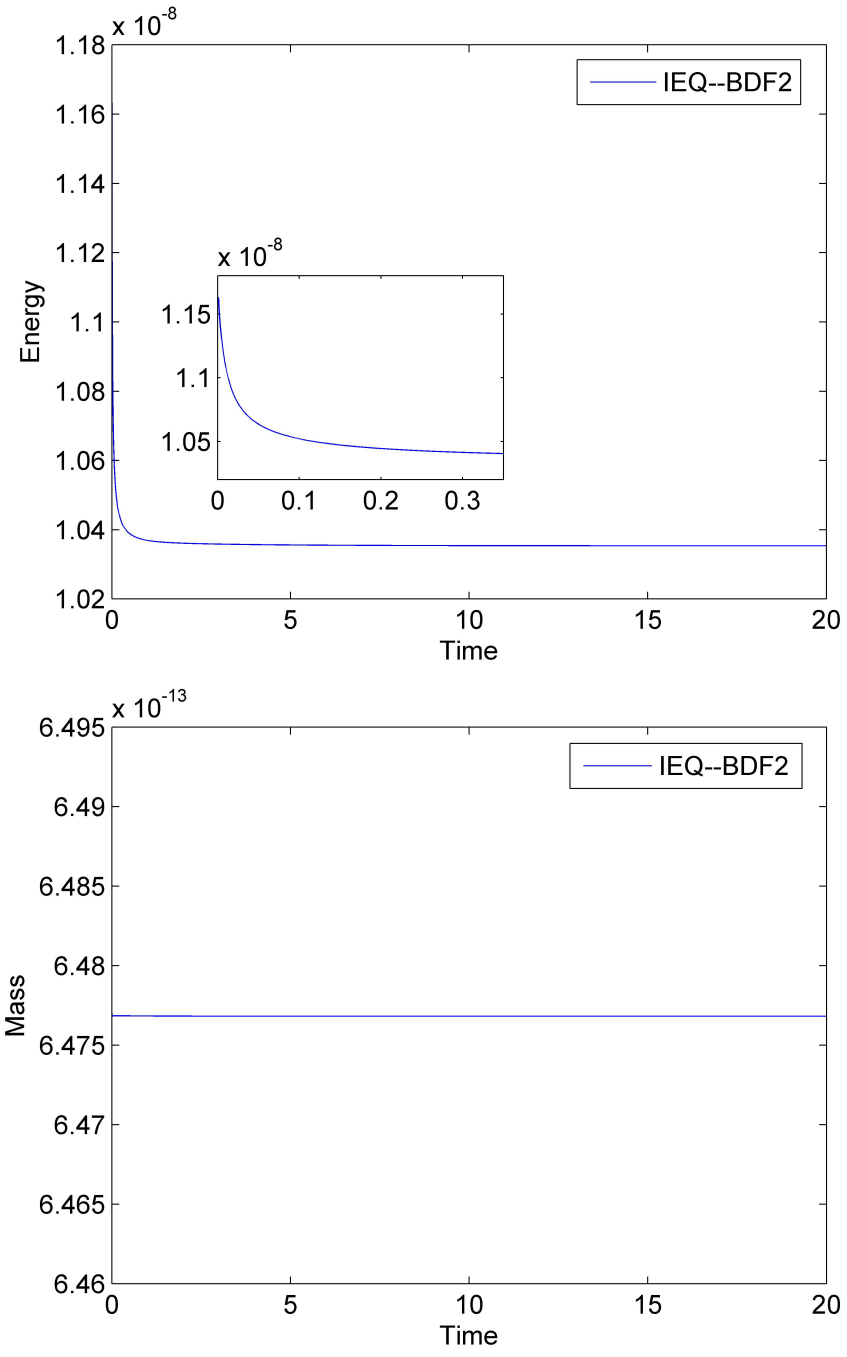

Figure 5.3 Energy and mass evolutions of one droplet in 2D. Top: energy; Bottom: mass.

FOUR DROPLETS

Next, we simulate the dynamical evolution of the molar density distribution for the case of having four droplets in the initial configuration – the liquid density of isobutane under a saturated pressure condition at the temperature 350K is imposed in the subregion of four squares $\left\{\left(\frac{L}{4}, \frac{L}{2}\right), \left(\frac{5L}{8}, \frac{7L}{8}\right)\right\}^2$, and the rest of the domain is filled with a saturated gas of isobutane under the same temperature. Figure 5.4 presents the simulated molar density distribution of Helmholtz free energy density for the case of four droplets at different times (t = 0, 5,10, 20, 40, 50, respectively) during the evolution, and Figure 5.5 the surface tension contribution of Helmholtz free energy density at the same times. The steady state seems reached at the time $t = 50$, which is longer than that needed for the single droplet case. We observe that the shapes of the four droplets are square initially, then four corners of all droplets are slowly rounded to become four circles as the time increases, and next the four circular droplets start to merge together and finally form one bigger circle. Figure 5.6 plots the evolution of the total energy and the mass, and again it is observed that the energy decreases monotonically and the mass is accurately maintained along the time. We also observe that there is a quite large energy decay at the very early time and small energy decay thereafter before steady state is reached.

We remark that extra experiments with a smaller time step size $\Delta t = 0.001$ and a larger penalty parameter P = 1.0E+21 for the above examples are also carried out to make sure the convergences of the numerical solutions, and very similar simulation results are obtained for both one and four droplets cases.

5.1.3 3D SIMULATION

Now we carry out some experiments to simulate the dynamics of the molar density distribution in 3D. We use the IEQ-BDF2 scheme with Δt = 5.0E-3 and a uniform mesh of $128 \times 128 \times 128$ and set the penalty parameter P = 1.0E+30.

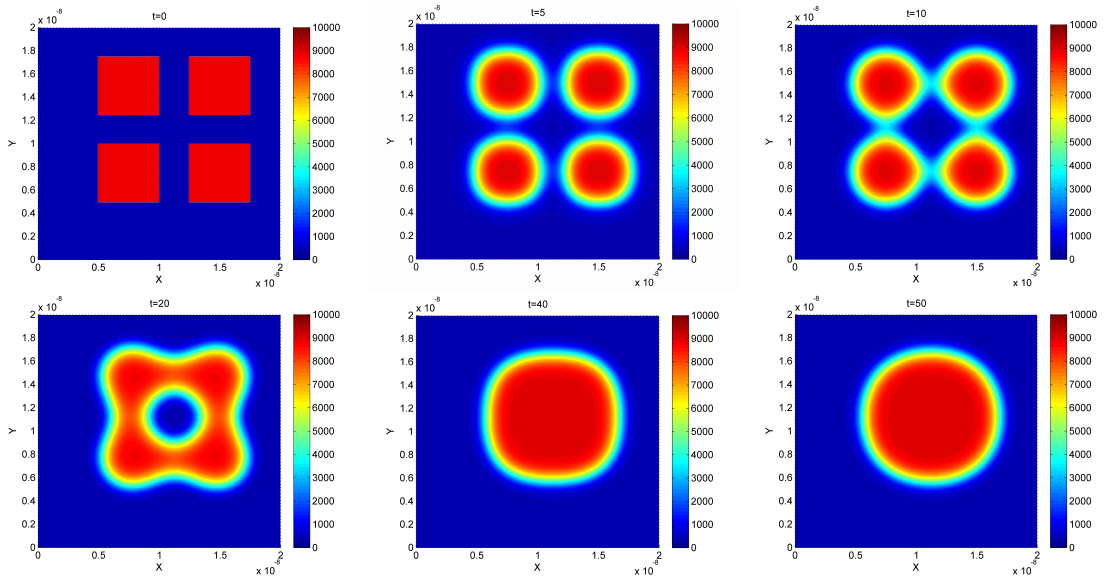

Figure 5.4 Dynamical evolution of four droplets in 2D: molar density distribution of C_4H_{10}.

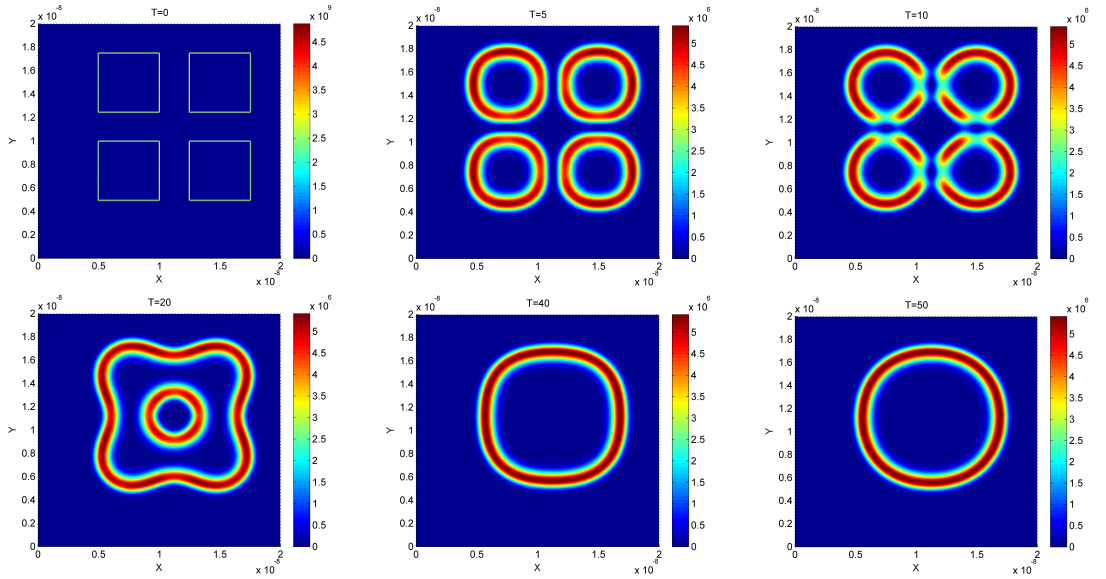

Figure 5.5 Dynamical evolution of four droplets in 2D: surface tension contribution of Helmholtz free energy density of C_4H_{10}.

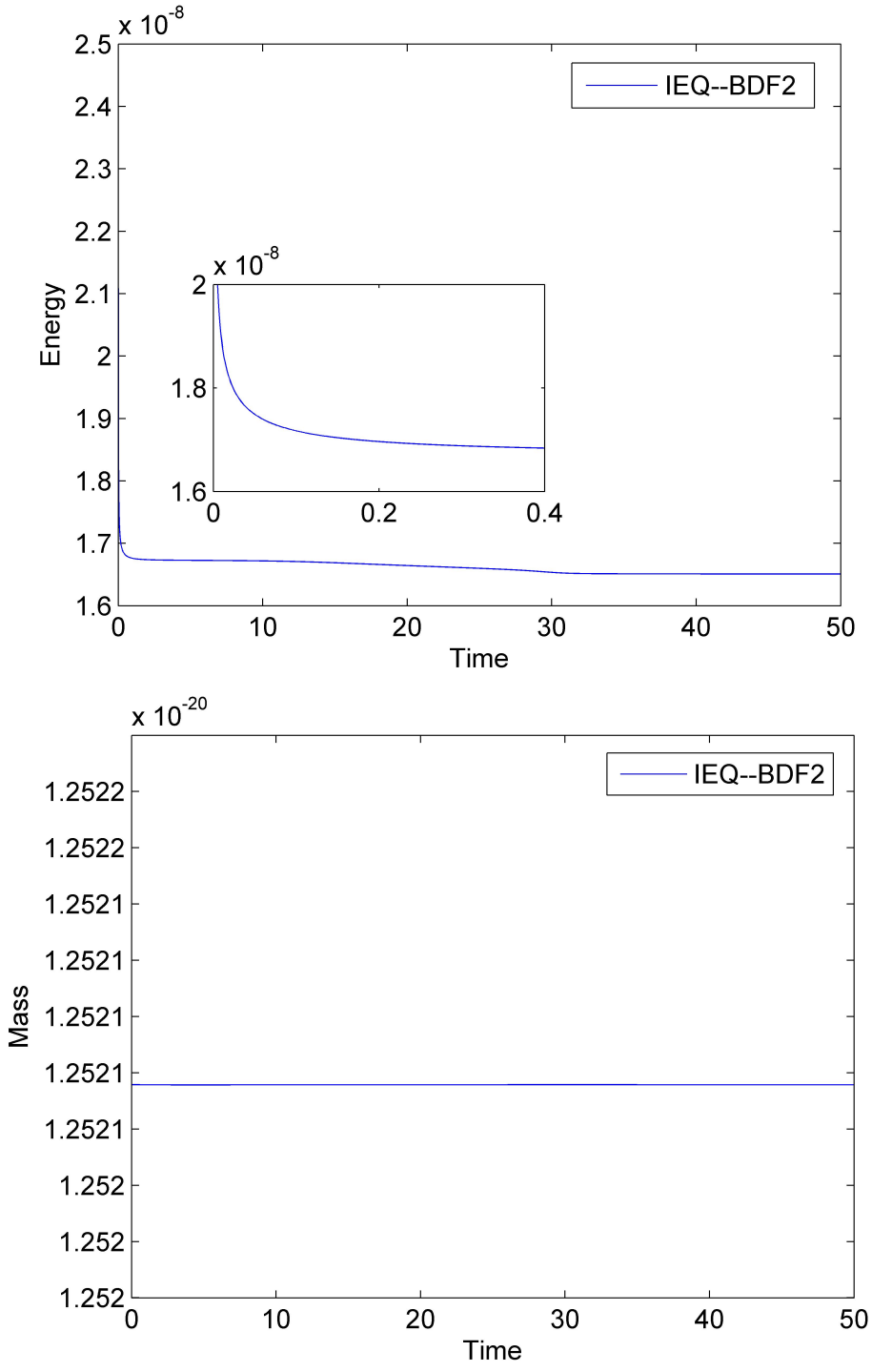

Figure 5.6 Energy and mass evolutions of four droplets in 2D. Top: energy; Bottom: mass.

ONE DROPLET

We first test using a single droplet as the initial condition – the liquid density of isobutane under a saturated pressure condition at the temperature $350K$ is imposed in the cube subregion of $(\frac{3L}{8}, \frac{3L}{4})^3$, and the rest of the cube is filled with a saturated gas of isobutane under the same temperature. Figure 5.7 presents the simulated molar density distribution for one droplet in 3D at different times (t = 0, 1, 3, 5, 10, 20, respectively) during the evolution. In each time panel, the top one represents the isosurface and the bottom one represents the approximated solution across the three central planes of the 3D cubic domain. We observe that the 3D dynamical behaviors are very consistent with 2D cases, and the droplet finally forms a perfect sphere around the time $t = 20$, which is almost the steady state. Figure 5.8 plots the evolution of total energy and the mass along the time, and we again observe that the energy monotonically decays and the mass are well preserved with respect to time.

EIGHT DROPLETS

For the next example in 3D, the initial configuration is taken to be eight droplets – the liquid density of isobutane is imposed in the subregion of eight cubes $\left\{\left(\frac{L}{4}, \frac{L}{2}\right), \left(\frac{5L}{8}, \frac{7L}{8}\right)\right\}^3$ at $350K$, and the rest of the domain is filled with a saturated gas of isobutane under a saturated pressure condition at the same temperature. Figure 5.9 presents the simulated molar density distribution for the eight droplet case in 3D at different times ($t = 0, 5, 10, 20, 40, 50$, respectively) during the evolution. The eight cubic droplets first evolve into eight separate spheres, then start to merge and finally form one bigger sphere around the time $t = 50$. This dynamic process is very similar to that for the four droplets case in 2D. In Figure 5.10, we present the evolution of the total energy and the mass with respect to the time, and observe again that the energy monotonically decays and the mass always keeps constant.

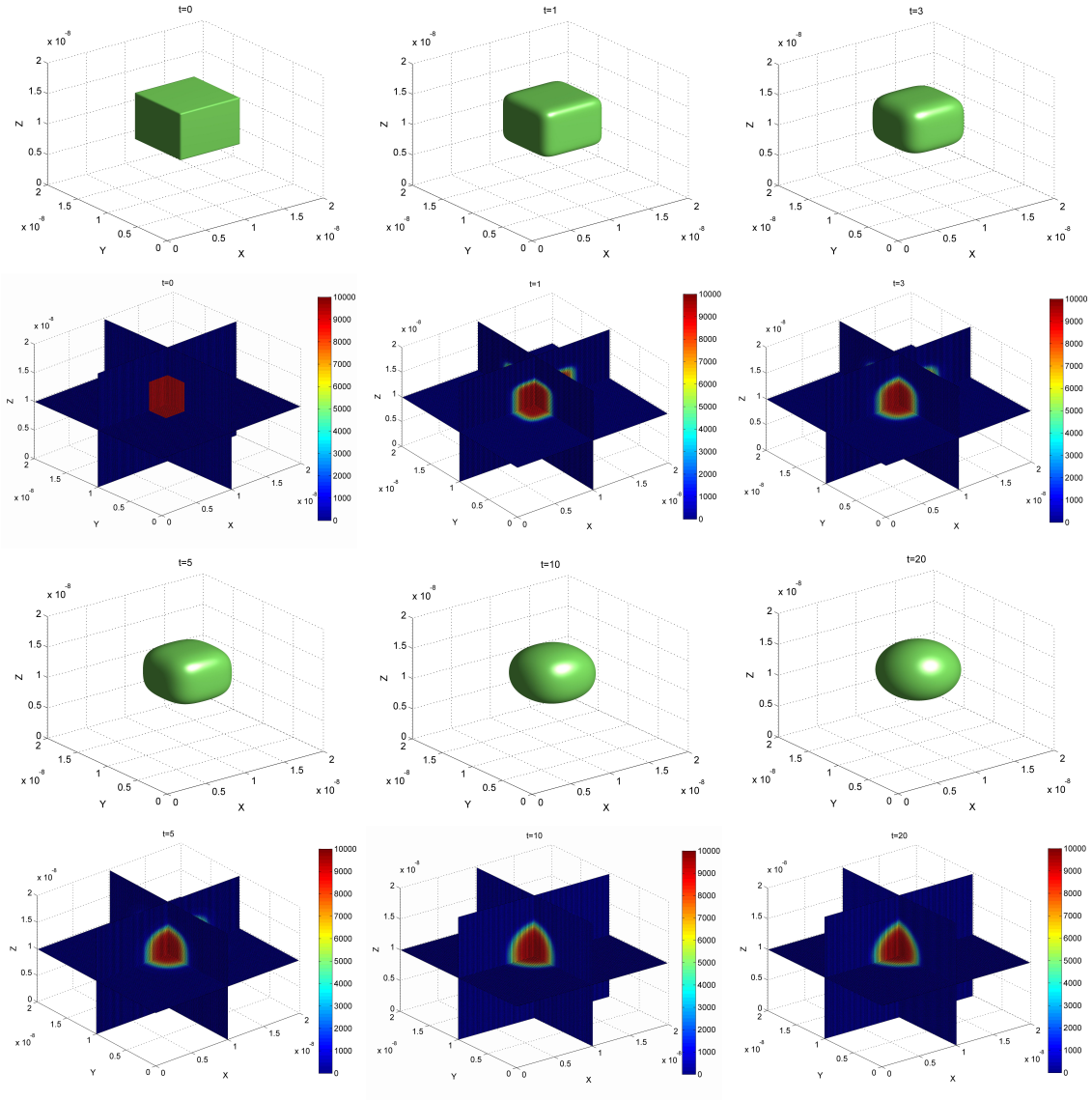

Figure 5.7 Dynamical evolution of one droplet in 3D: molar density distribution of C_4H_{10}.

5.1.4 Comparisons with laboratory data

We now compare the numerical predictions from our simulations with laboratory data to valid the reliability of our schemes. As the quantity of interest in many applications, the surface tension σ is defined as the work for creating a unit area of interface with a unit of J/m^2 or the net contractive force per unit length of interface

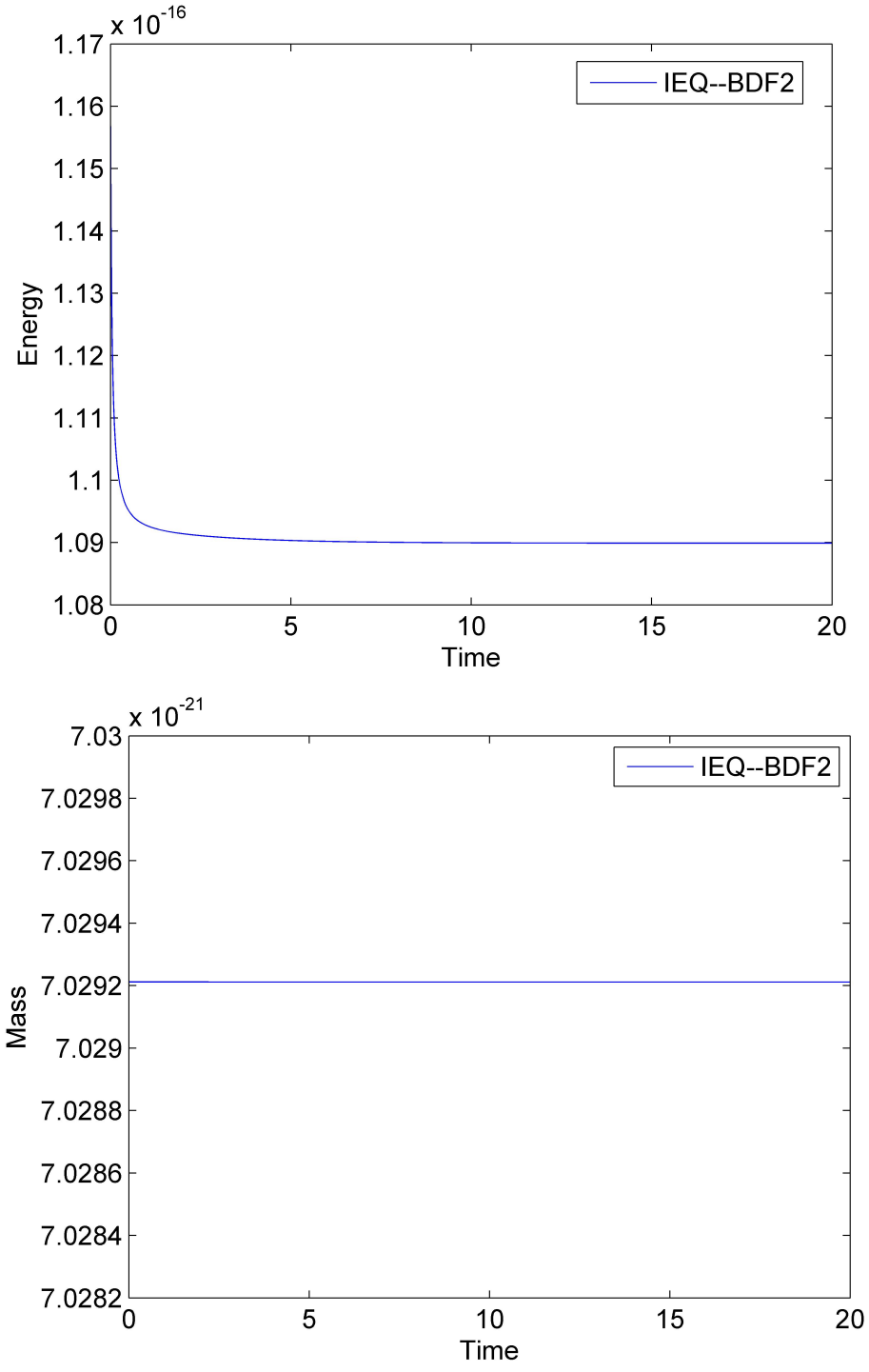

Figure 5.8 Energy and mass evolutions of one droplet in 3D. Top: energy; Bottom: mass.

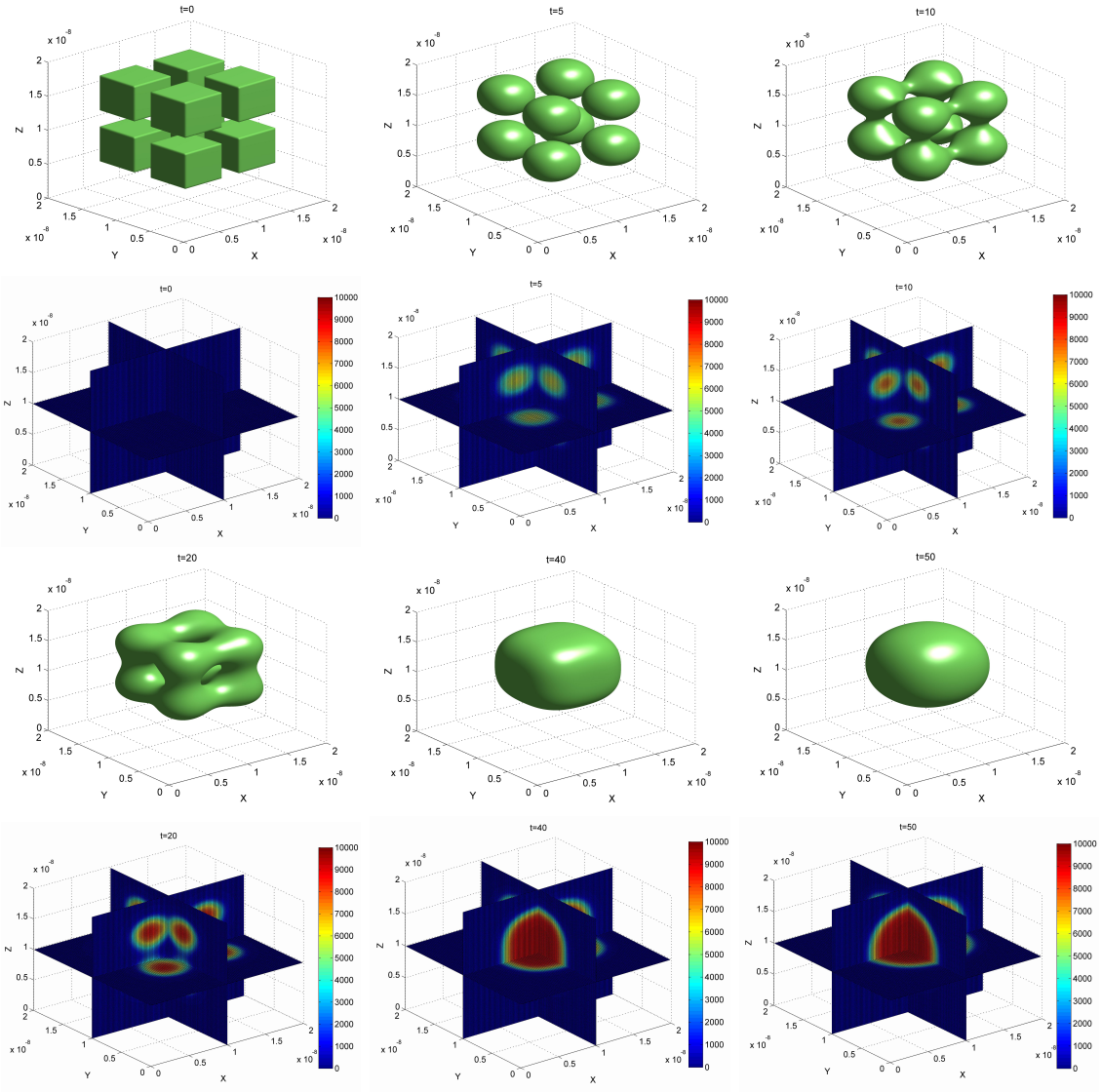

Figure 5.9 Dynamical evolution of eight droplets in 3D: molar density distribution of C_4H_{10}.

with a unit of N/m from the thermodynamical or mechanical point of view. In this model, the surface/interface tension σ is defined by

$$\sigma = \frac{\partial F}{\partial A} = \frac{F(n) - F_0(n_{initial})}{A} \cong \frac{\int_\Omega f_{ST} d\mathbf{x}}{A},$$

where A is the area of the interface.

Let us assume that the mass of the liquid droplet does not change along with time and the steady state droplet has a perfect circular/spherical shape. For the single

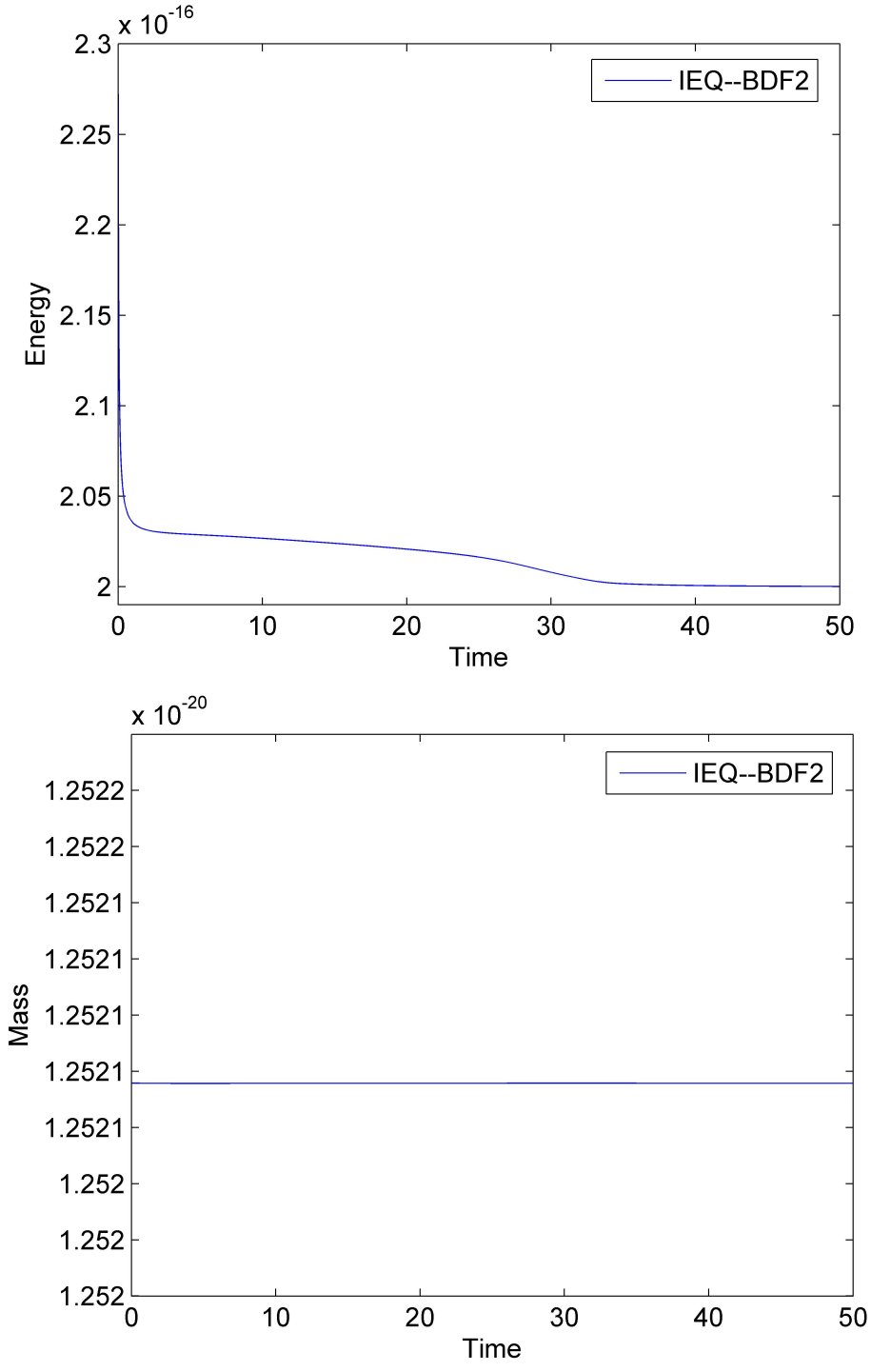

Figure 5.10 Energy and mass evolutions of eight droplets in 3D. Top: energy; Bottom: mass.

droplet case in 2D, the radius of the circular droplet is $r = 4.231 \times 10^{-9}$ meters. The surface tension of isobutane in the equilibrium state at the temperature ranging from 250K to 333.82K are calculated by using the IEQ-BDF2 scheme with $\Delta t =$ 5.0E-3 on the uniform mesh of 512×512 and the penalty parameter $P =$ 1.0E+20. For example, $F(n) - F_0(n_{initial}) \cong 2.229 \times 10^{-10} J$ at the temperature $T = 333.82$K, and the corresponding interface tension is $\sigma = 8.384 \times 10^{-3} J/m^2$ by our simulation. The complete results are presented in left panel of Figure 5.11 together with the laboratory measured values provided in [32]. It is clear that the differences between the numerical results and the experimental data is small from the engineering point of view.

Based on the values of the surface tension, we can test another physically concerned quality, the capillary pressure P_c, which defined by the well-known Young-Laplace equation

$$P_c = P_{liquid} - P_{gas} \approx \frac{\sigma}{r}, \tag{5.2}$$

where the thermodynamic pressure for the liquid P_{liquid} or the gas P_{gas} is defined by

$$P = \frac{nRT}{1 - bn} - \frac{n^2 a(T)}{1 + 2bn - b^2 n^2}. \tag{5.3}$$

According to the equation (5.2), there are two different ways to numerically calculate the capillary pressure, one is to use the difference between the liquid drop pressure and the pressure of the gas phase and the other is to use the numerical results obtained for the interface tension σ. For example, at the temperature 333.28K, $P_{liquid} = 2.634 \times 10^6$Pa and $P_{gas} = 0.701 \times 10^6$Pa, thus the difference is $P_c = 1.933 \times 10^6$Pa. On the other hand, the capillary pressure obtained from the approximated interface tension is $P_c = \frac{\sigma}{r} = 1.981 \times 10^6$Pa. It is clear that the Young-Laplace prediction is well matched with the capillary pressure obtained by our numerical schemes with about an error of 2%. The right panel of Figure 5.11 plots the capillary pressure from 250K to 333.82K, which are calculated by above two ways. The matching errors are all

about or smaller than 2% at tested temperatures. In this case, the diffuse interface model with Peng-Robinson equation of state and the proposed numerical schemes are physically reliable to be used to simulate the two-phase fluid of the substance isobutane.

We next use the results from the single droplet case in 3D to compare with the laboratory data. The IEQ-BDF2 scheme with Δt = 5.0E-3 on the uniform mesh of $128 \times 128 \times 128$ and the penalty parameter P = 1.0E+30 is used for all simulations, and the results are given in Figure 5.12. The simulated interface tensions at all tested temperatures still match the laboratory data from the engineering point of view. For the capillary pressure, the results calculated from the Young-Laplace equation are close to those obtained from the approximate interface tensions when the temperature is in the high end of the $[250, 333.28]$, but the difference becomes larger and larger along with the decreasing of the temperature. This issue on the capillary pressure may be worthy of further investigation from the modeling side on the causes.

5.2 Multi-component system

5.2.1 Temporal accuracy test

In order to test the convergence order, we first use the case of one single droplet, that is, the liquid density of the mixture consisting of isobutane (C_4H_{10}) and decane ($C_{10}H_{22}$) under a saturated pressure condition at the temperature 450K is imposed in a square subregion $(\frac{3L}{8}, \frac{5L}{8})^2$, and the rest of domain is filled with a saturated gas of the mixture under same temperature. We perform our simulations on the time interval $t0.6$ with refinement time step size $\Delta t = 2.0\text{E}-2, 1.0\text{E}-2, \cdots, 3.125\text{E}-4$ for both the first order (IEQ-1) and the second order (IEQ-BDF2) schemes. We choose the stabilizer coefficients $\kappa_i = 180$, together with a lower bound 1E+12 and use a 256×256 mesh grid in 2D. We compare each simulated solution with the benchmark obtained by each scheme with Δt = 1.0E-5. The L^2 relative errors and convergence

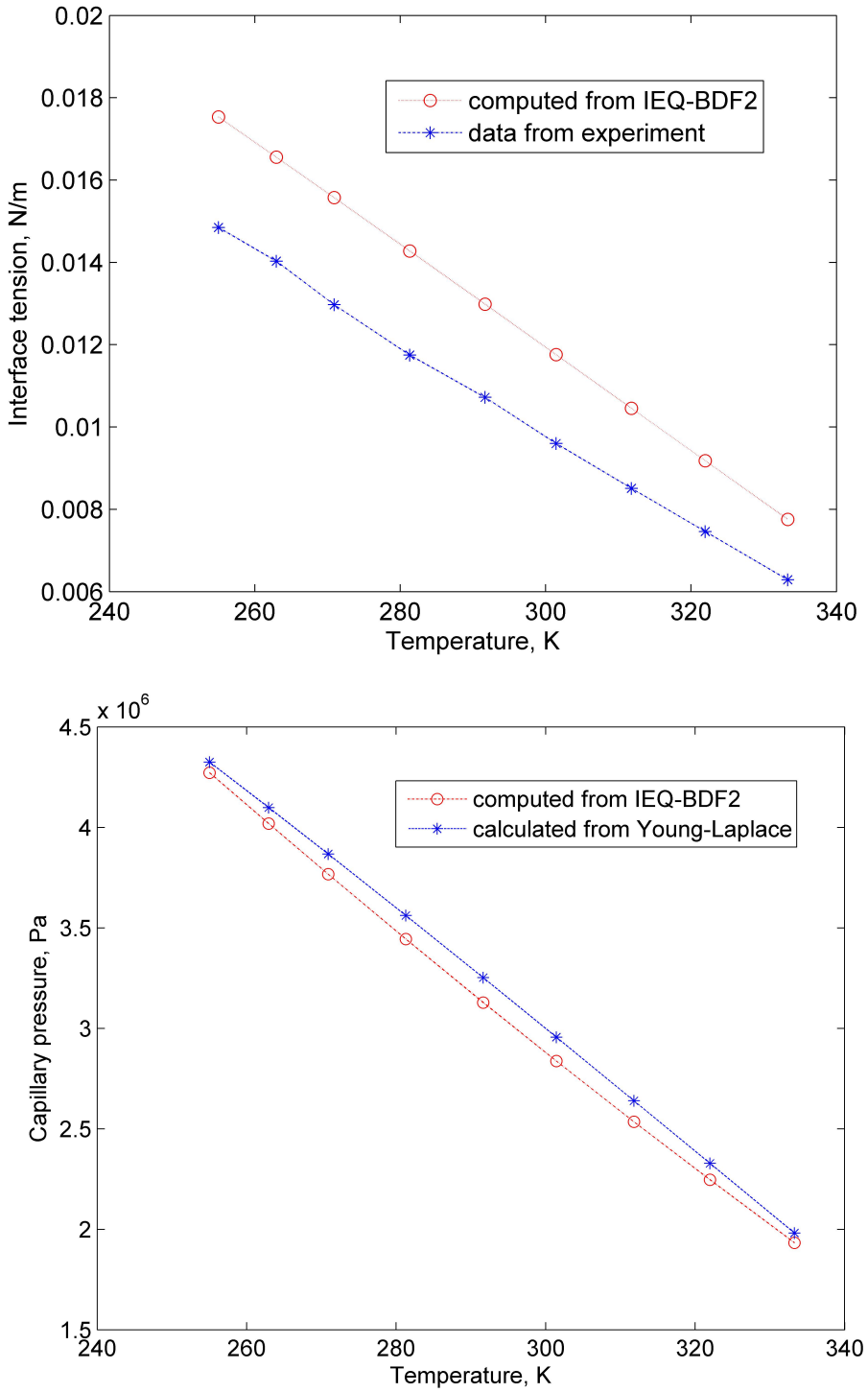

Figure 5.11 Comparison between the numerical predictions and the laboratory data in 2D. Top: interface tension; Bottom: capillary pressure.

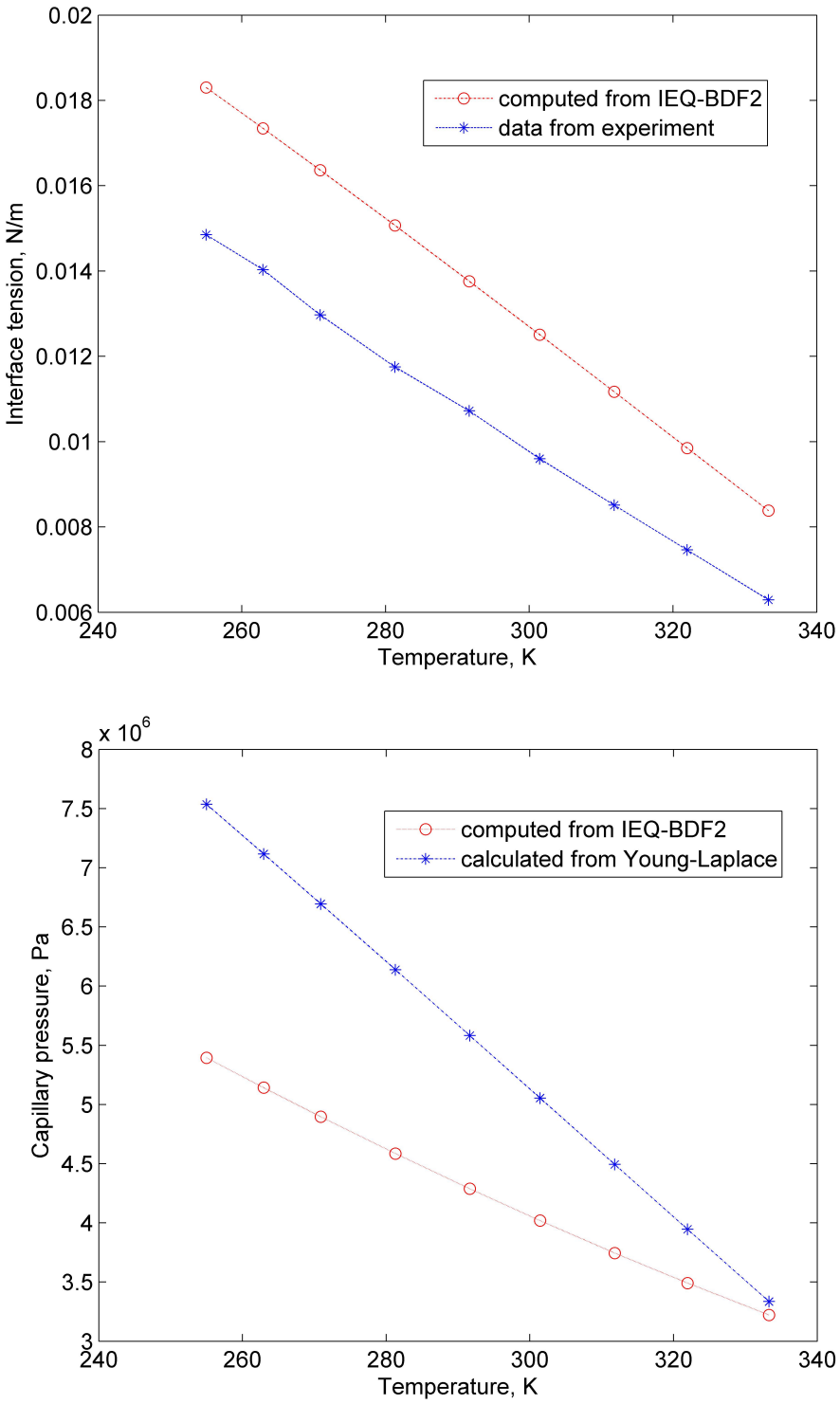

Figure 5.12 Comparison between the numerical predictions and the laboratory data in 3D. Top: interface tension; Bottom: capillary pressure.

rates are listed in Table 5.3.

Table 5.3 Convergence tests for multi-component system.

Time Step Size Δt	IEQ-1		IEQ-BDF2	
	Error	Conv. Rate	Error	Conv. Rate
2.0E-2	2.1943E-2	-	1.5156E-2	-
1.0E-2	1.8201E-2	0.27	5.9916E-3	1.34
5.0E-3	1.3570E-2	0.42	1.6472E-3	1.86
2.5E-3	8.9856E-3	0.59	4.4788E-4	1.88
1.25E-3	5.3502E-3	0.75	1.2479E-4	1.84
6.25E-4	2.9414E-3	0.86	3.4321E-5	1.86
3.125E-4	1.5298E-3	0.94	9.1366E-6	1.91

From Table 5.3, it is easy to observe that both the IEQ-1 and IEQ-BDF2 schemes are very stable for all time step sizes, and have almost first and second order accuracy, respectively.

5.2.2 2D simulation

In this section, we investigate the time evolution of the molar density distribution and the gas-liquid interface in 2D with one droplet and four droplets, respectively. The IEQ-BDF2 scheme with Δt=5.0E-3 is adopted to perform the simulations. The stabilizer coefficients, the lower bound and the mesh grid are chosen as $\kappa_i = 180$, 1.0E+12 and 256×256, respectively.

one droplet

The liquid density of the mixture is filled in the square subdomain of $(\frac{3L}{8}, \frac{5L}{8})^2$, and a saturate gas of both components is full of the rest of the domain under the temperature 450K. The simulations of evolution process are shown in Figure 5.13 and Figure 5.14 at different times ($t = 0, 0.5, 1, 2, 5, 10$) for both components, isobutane and decane, respectively. We can observe that the shape of the droplet for the liquid phase is initially square, then corners are rounded and turning to a circle as system

approaching to steady state, and finally the droplet becomes a perfect circle. This coincides with Figure 5.15 where the energy decreasing is significant at the beginning and slows down as density of each substance is distributed uniformly in all directions and a circular interface is formed, and the mass conservation is well preserved.

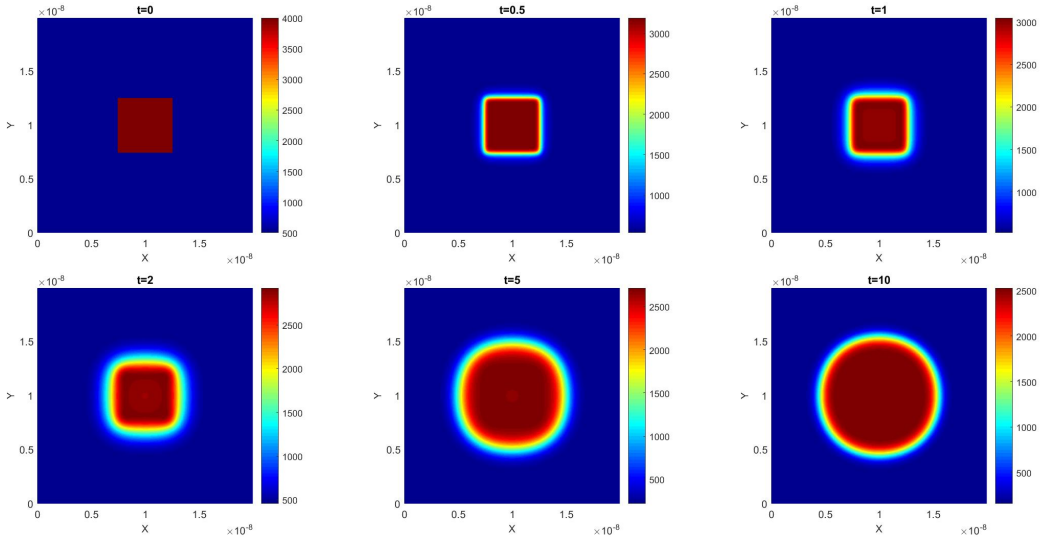

Figure 5.13 Dynamical evolution of one droplet in 2D: molar density distribution of C_4H_{10}.

FOUR DROPLETS

Next, we simulate the dynamical evolution of molar density distribution for the case of having four droplets as initial configuration, that is, the liquid density of the mixture under a saturated pressure condition at the temperature 450K is imposed in the square subregion of $\{(\frac{3L}{16}, \frac{7L}{16}), (\frac{9L}{16}, \frac{13L}{16})\}^2$, and the rest of domain is filled with a saturated gas of the mixture under same temperature. The simulation of evolution process are shown in Figure 5.16 and Figure 5.17. We observe that the shapes of four droplets are initially square, then four corners are slowly rounded to become circular. Next when the interfaces of droplets start to touch each other, these four droplets start to merge to form one circle-like droplet. In Figure 5.18 we plot the evolutions

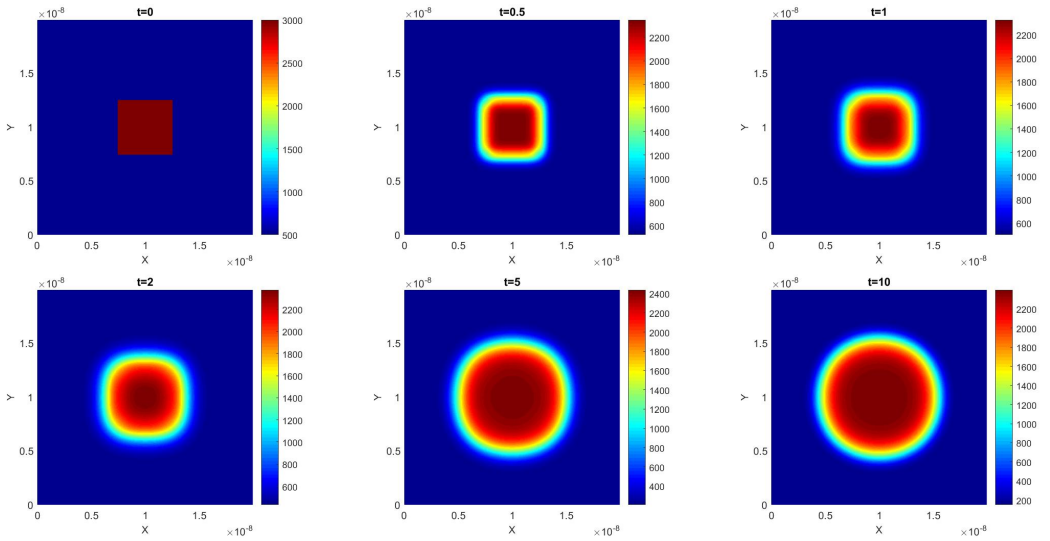

Figure 5.14 Dynamical evolution of one droplet in 2D: molar density distribution of $C_{10}H_{22}$.

of total energy and mass, and again observe that the energy decreases monotonically and the mass of each species is accurately maintained along the time.

5.2.3 3D SIMULATION

Experiments are presented to simulate the dynamics of the molar density distribution of both components in 3D. We adopt the IEQ-BDF2 scheme with Δt=5.0E-3 and a uniform mesh of $128 \times 128 \times 128$ grid together with a lower bound 1.0E+12 and the stabilizer coefficients $\kappa_i = 180$.

ONE DROPLET

The first simulation has a single droplet as the initial condition. The liquid density of the mixture under a saturated pressure condition at the temperature 450K is imposed in the cube subregion of $(\frac{3L}{8}, \frac{5L}{8})^3$, and the rest of the cube is filled with a saturated gas of both components under the same temperature .

Figure 5.19 and Figure 5.20 present the simulated molar density distribution for

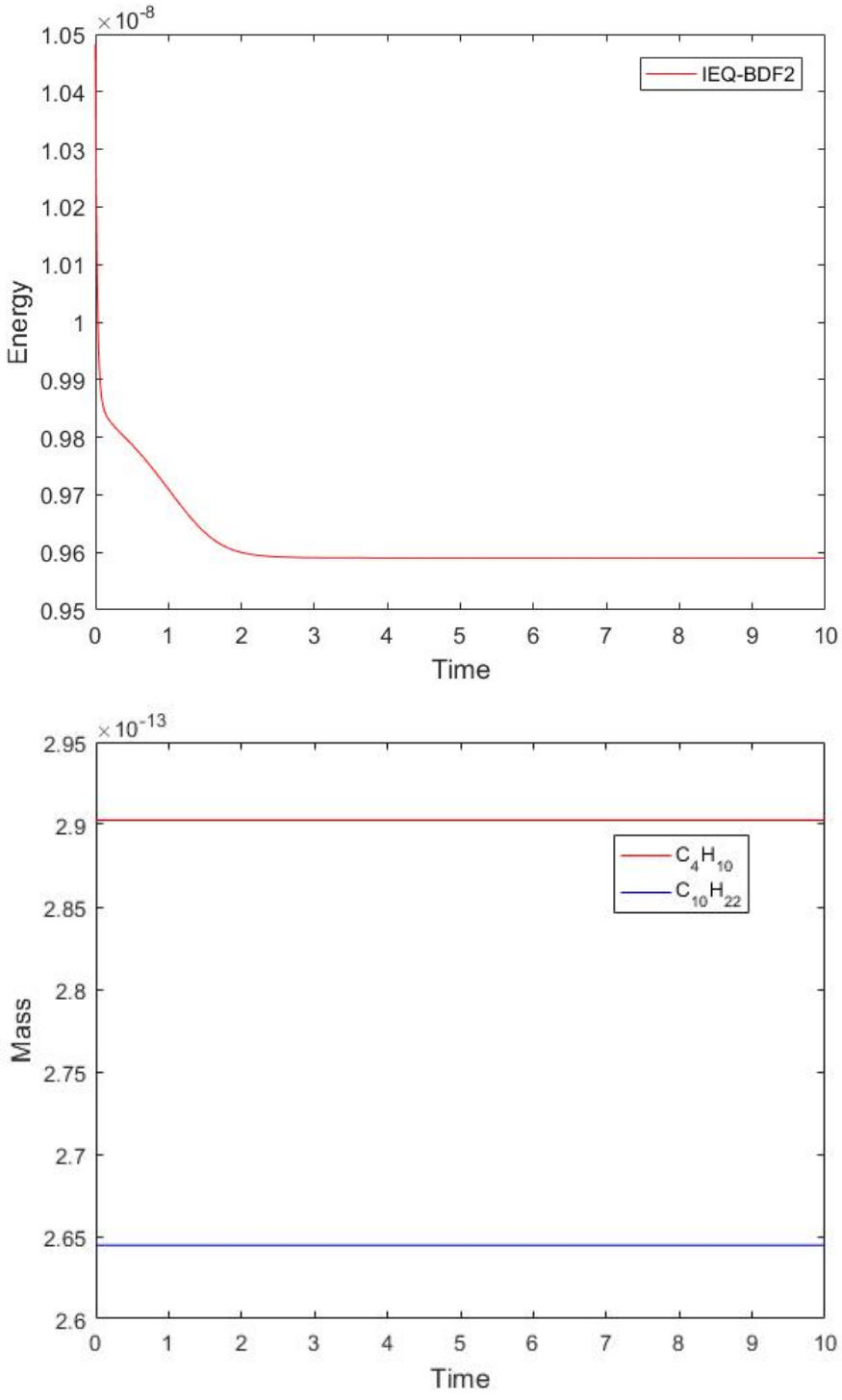

Figure 5.15 Energy and mass evolutions of one droplet in 3D. Top: energy; Bottom: mass.

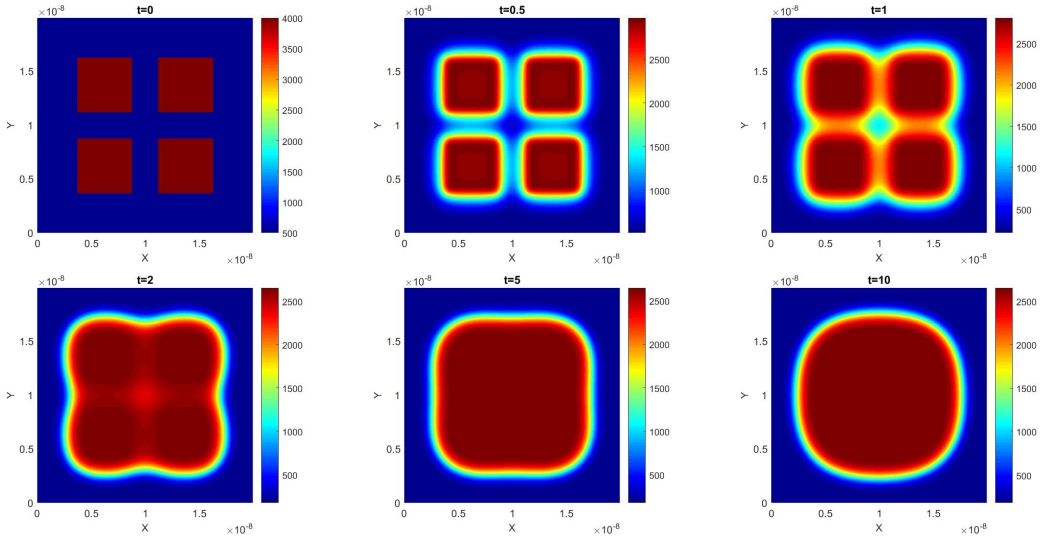

Figure 5.16 Dynamical evolution of four droplets in 2D: molar density distribution of C_4H_{10}.

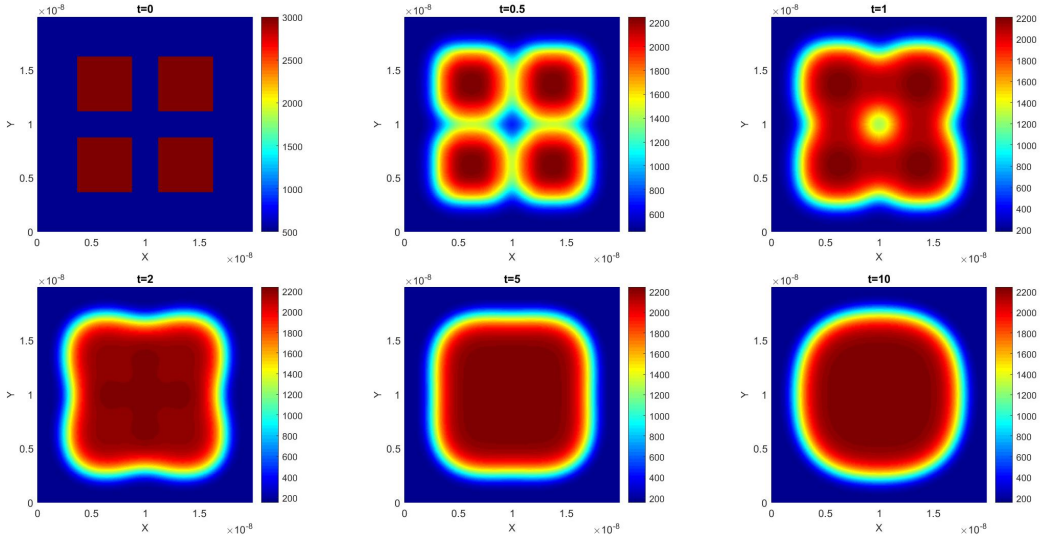

Figure 5.17 Dynamical evolution of four droplets in 2D: molar density distribution of $C_{10}H_{22}$.

both components in 3D at different times ($t = 0, 0.5, 1, 2, 5, 10$) during the evolution, respectively. Similar to the dynamical behaviors of a single droplet in 2D, we can observe that the droplet finally forms a sphere and the steady state is reached. The

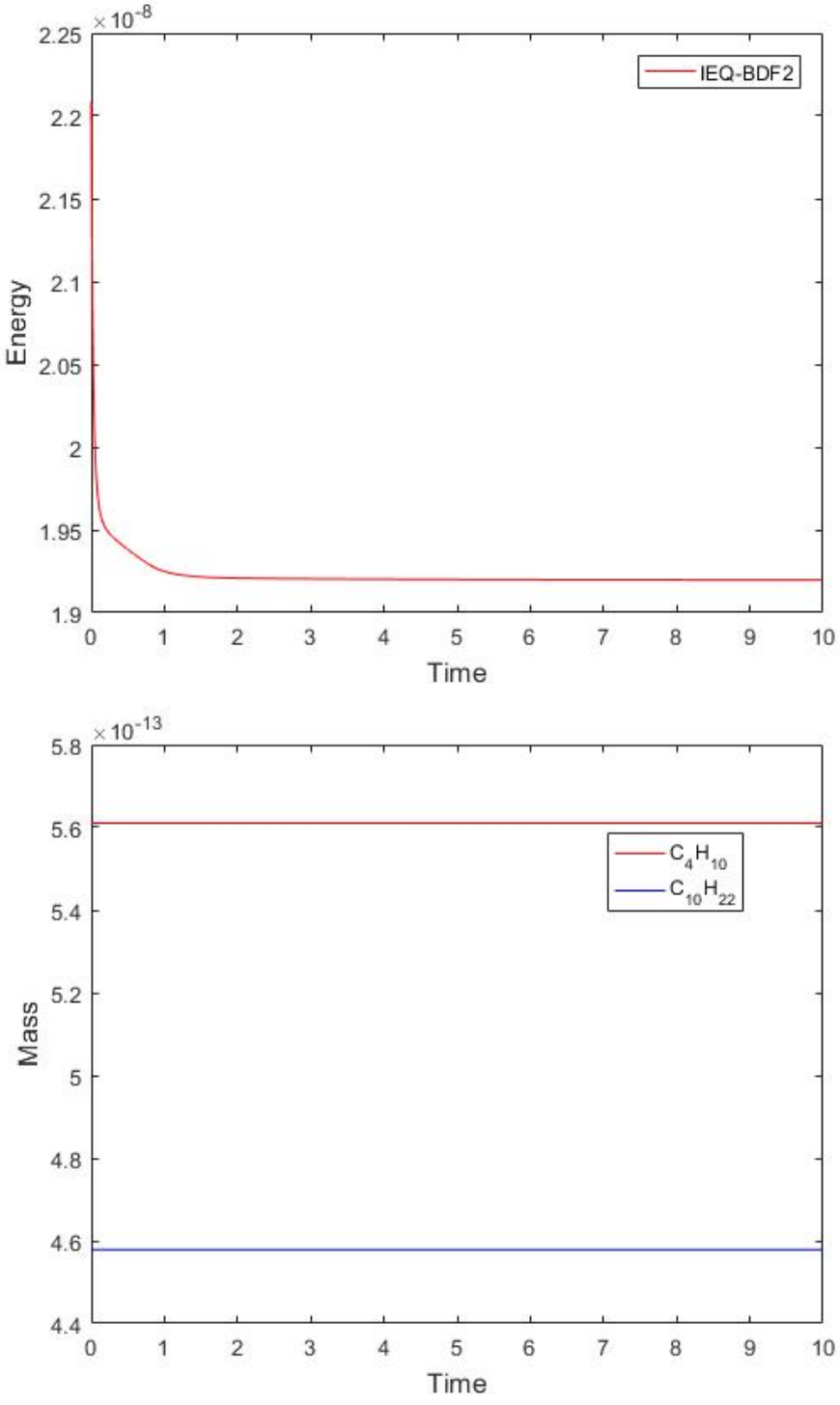

Figure 5.18 Energy and mass evolutions of four droplets in 2D. Top: energy; Bottom: mass.

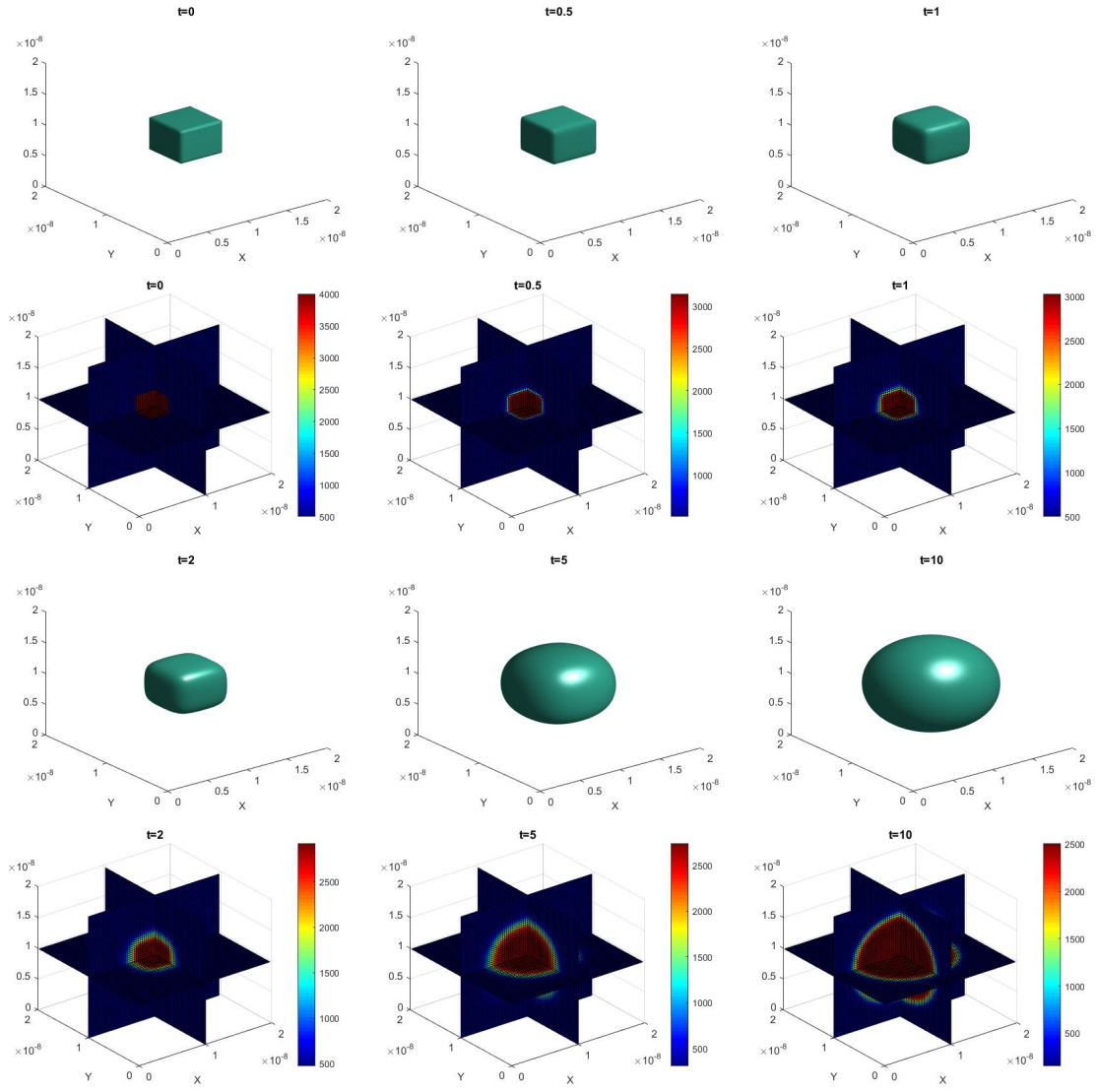

Figure 5.19 Dynamical evolution of one droplet in 3D: molar density distribution of C_4H_{10}.

evolutions of the total energy and the mass are plotted in Figure 5.21. We can see that the energy decreases monotonically and the masses are accurately maintained along the time. Furthermore, there is a quite large energy decay at the beginning.

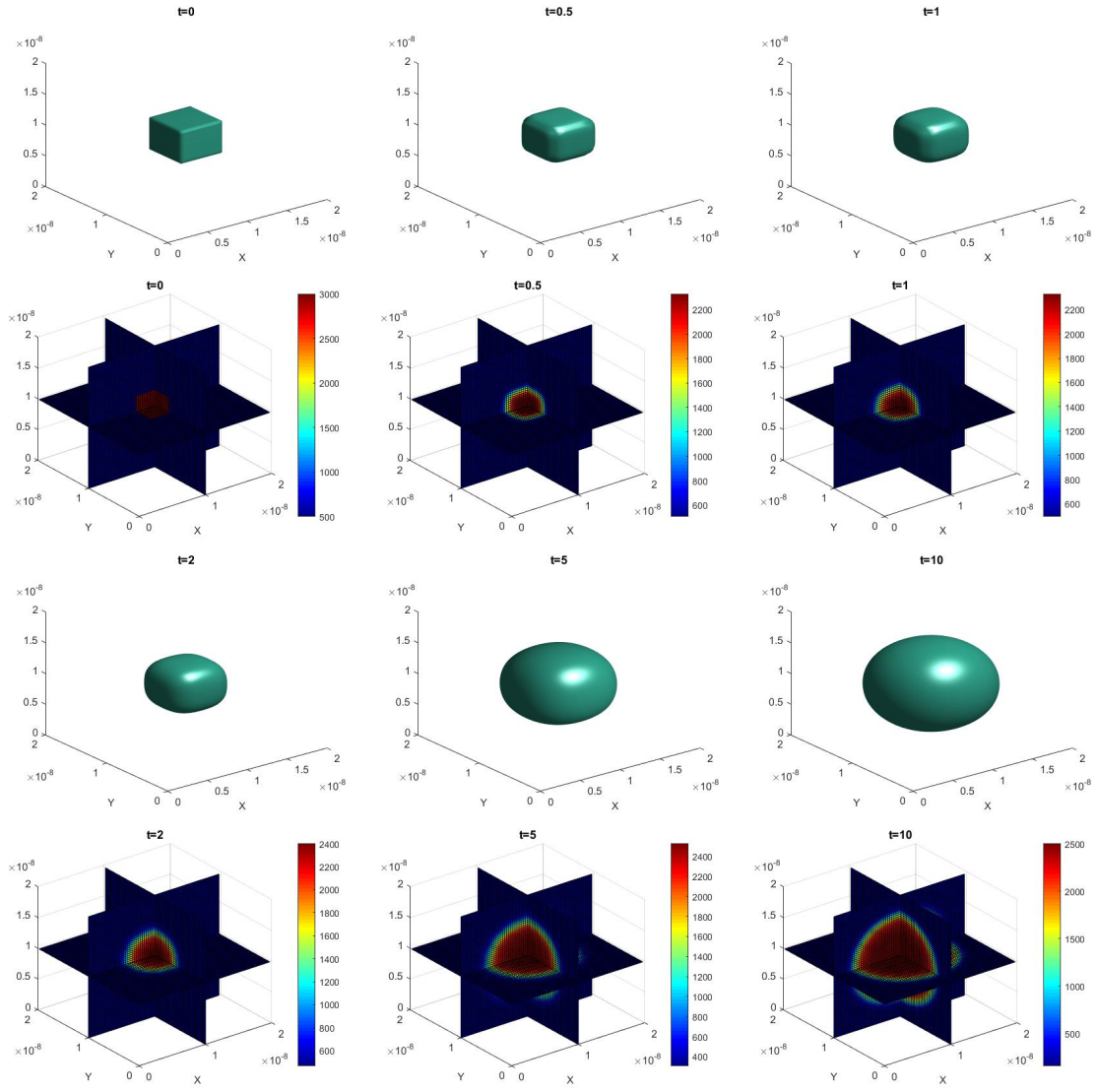

Figure 5.20 Dynamical evolution of one droplet in 3D: molar density distribution of $C_{10}H_{22}$.

EIGHT DROPLETS

For the initial condition, the liquid density of both components under a saturated pressure condition at the temperature 450K is imposed in the cube subregion of $\{(\frac{3L}{16}, \frac{7L}{16}), (\frac{9L}{16}, \frac{13L}{16})\}^3$, and the rest of the cube is filled with a saturated gas of the mixture under the same temperature.

The simulated molar density distributions for the mixture in 3D at different times

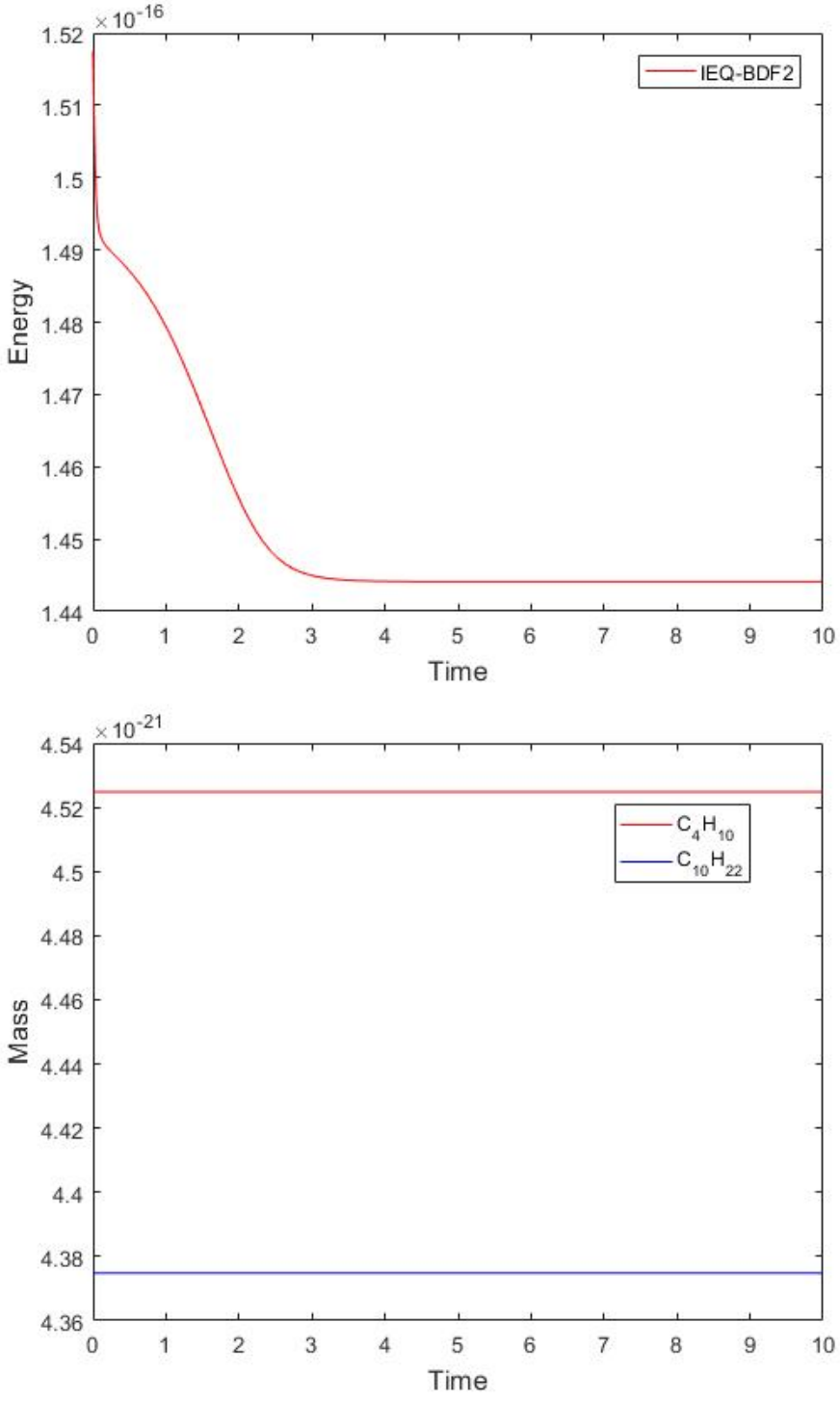

Figure 5.21 Energy and mass evolutions of one droplet in 3D. Top: energy; Bottom: mass.

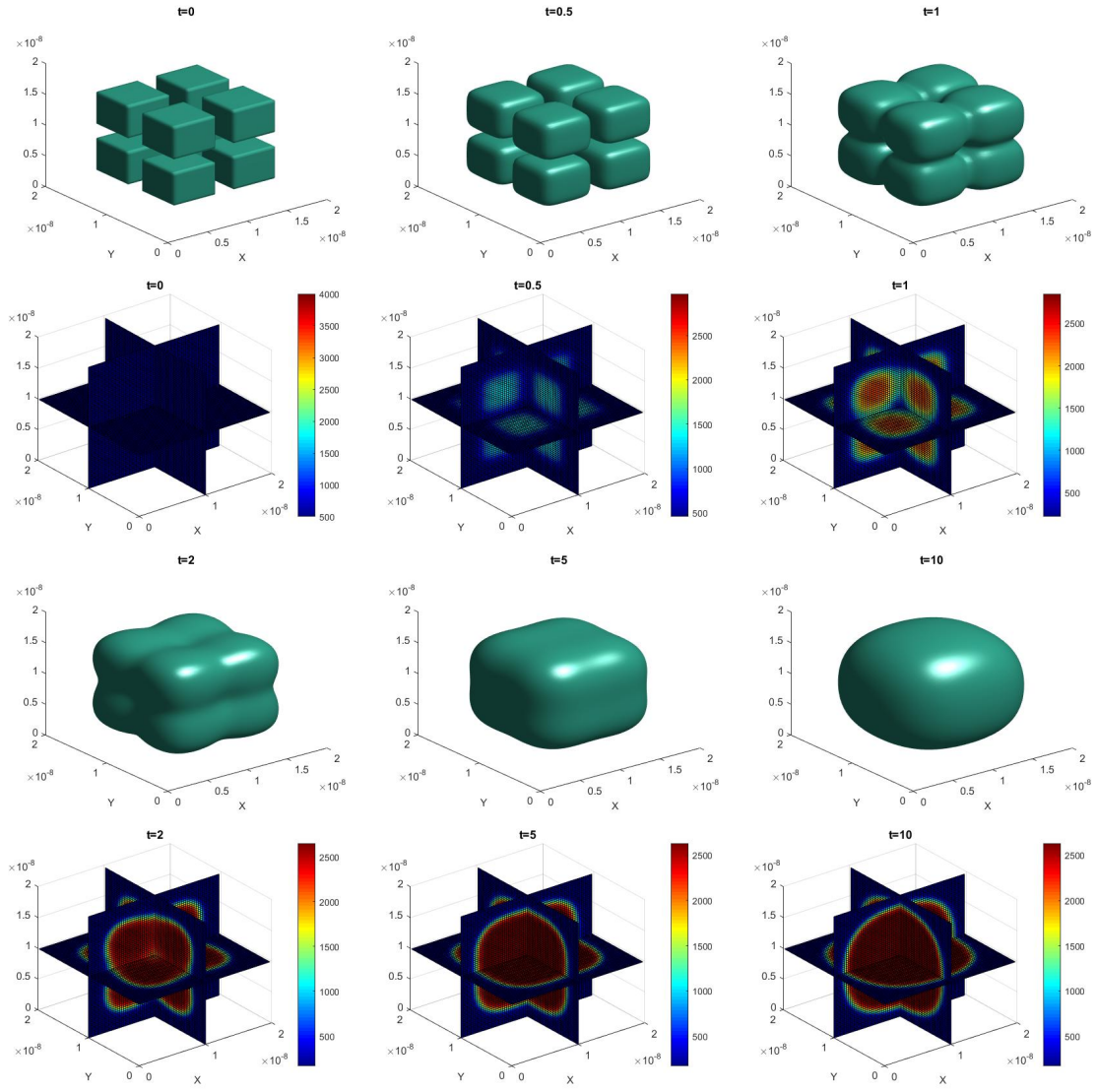

Figure 5.22 Dynamical evolution of eight droplets in 3D: molar density distribution of C_4H_{10}.

$(t = 0, 0.5, 1, 2, 5, 10)$ during the evolution are presented in Figure 5.22 and Figure 5.23. The eight droplets first form to eight separate spheres, then start to merge when their interfaces touch one another and finally become one bigger sphere in the steady state. The dynamical process is very consistent with that of the four droplets case in 2D. We present the evolution of the total energy and the mass with respect to the time in Figure 5.24, and observe again the energy monotonically decays and

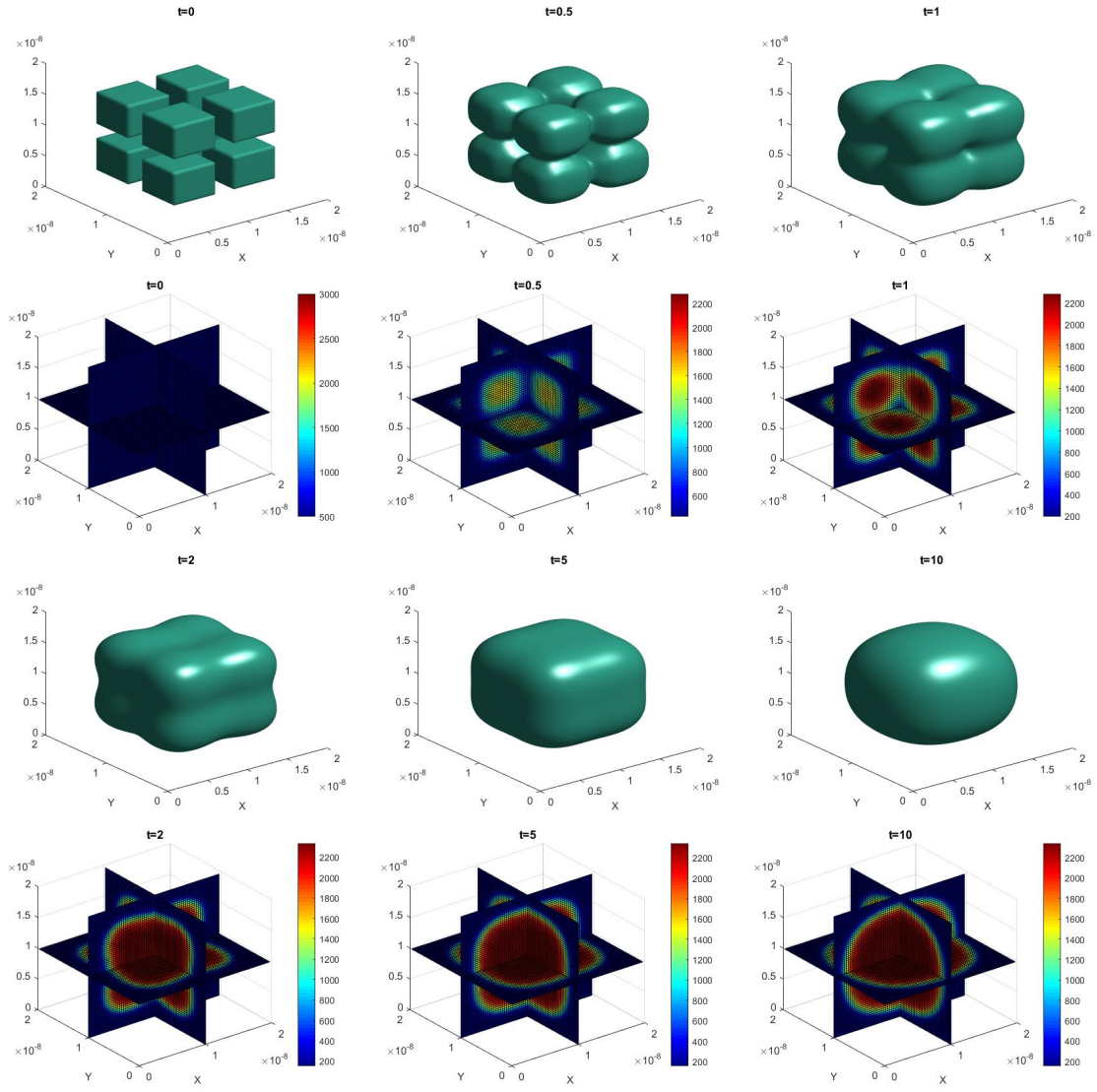

Figure 5.23 Dynamical evolution of eight droplets in 3D: molar density distribution of $C_{10}H_{22}$.

approaches an equilibrium state, and masses are accurately maintained along the time.

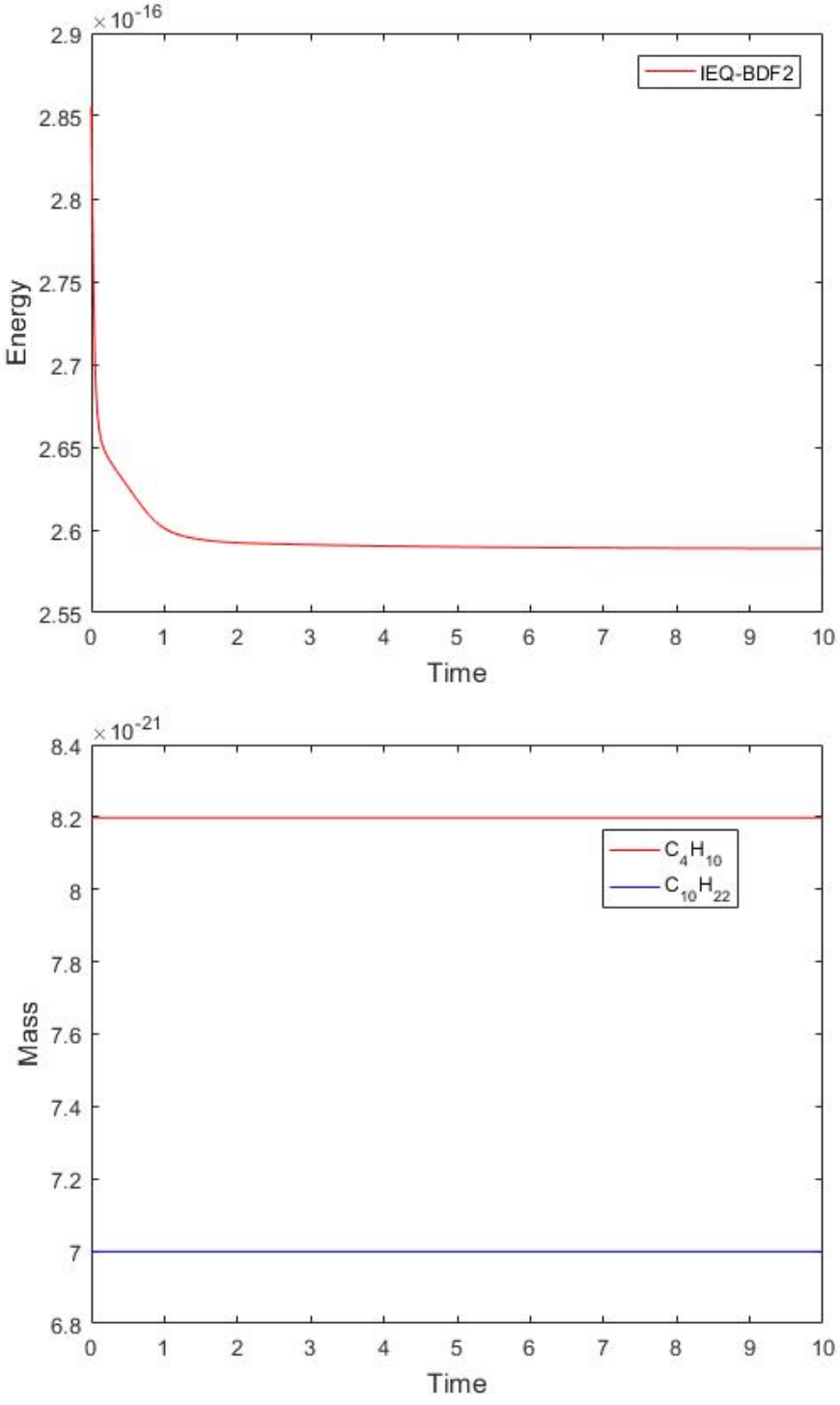

Figure 5.24 Energy and mass evolutions of eight droplets in 3D. Top: energy; Bottom: mass.

Chapter 6

Conclusions

In this dissertation, we design first and second order schemes for temporal discretization based on the IEQ approach to solve the diffuse interface model problems with Peng-Robinson equation of state. Single-component and multi-component two-phase fluid systems are specially considered. In particular, for multi-component system we introduce an orthonormal transformation in order to simplify the highly coupled systems, and combine the IEQ approach and stabilized method to solve the problem effectively. These schemes are accurate up to the second order, unconditionally energy stable, and easy to implement in practice. Moreover, the resulting linear systems in space at each time step are proven to be symmetric positive definite, so that one can implement the Krylov subspace methods to solve them efficiently. Numerical experiments in 2D and 3D spaces are also performed to demonstrate the accuracies and stabilities of the proposed schemes, and to investigate reliability of the target model by comparisons with laboratory data.

It is worthy to point out that since IEQ system is not strictly equal to the original system in the discrete sense, considering the dissipative energy in particular, it would not be an easy work to prove error estimates for the proposed numerical schemes as done for the convex-splitting method. This is an interesting open problem worthy of further investigation.

The IEQ method has proven to be a powerful approach to construct energy stable schemes. It is applicable to a large class of gradient flows [54, 57, 58, 59, 60, 61], and can be extended to higher-order BDF-k scheme, with BDF-2 being unconditionally

stable. However, there still exist some disadvantages in this approach. As illustrated in Chapter 3 and 4, for the semi-discretized systems at each time step, we need to solve linear equations with complicated variable coefficients, and we are using the fact that the free energy density is bounded from below, which may not hold for other physical models. In addition to that, for multi-component system, in order to have an efficient scheme, some efforts must be taken to decouple the relations in all components.

Based on IEQ method, Shen and his collaborators recently develop the scalar auxiliary variable (SAV) approach [44, 45]. It enjoys all advantages of the IEQ approach but overcomes most of its shortcomings mentioned here. For instance, instead of the quadratization of the energy density, the SAV approach introduce a scalar variable which leads to the quadratization of the energy functional, so it is applicable even if the energy density is not bounded from below. Moreover, it leads to linear systems with only constant coefficients at each time step, so that one can solve them with extreme efficiency. Therefore, it is worthy to design the unconditionally energy stable schemes for this diffuse interface model with Peng-Robinson equation of state by applying the SAV approach in a future work, and apply it to a large variety of gradient flows.

Bibliography

[1] D.M. Anderson, G.B. McFadden and A. A. Wheeler. Diffuse-interface methods in fluid mechanics. *Ann. Rev. Fluid Mech.*, 30: 139-165, 1998.

[2] V.E. Badalassi, H.D. Ceniceros and S. Banerjee. Computation of multiphase systems with phase field models. *J. Comput. Phys.*, 190: 371-397, 2003.

[3] Herbert B. Callen, and H. L. Scott, Thermodynamics and an Introduction to Thermostatistics, *American Journal of Physics*, 66, 164 (1998).

[4] C.M. Elliott, H. Garcke, On the Cahn-Hilliard equation with degenerate mobility, *SIAM J. Math. Anal.*, 27 (1996), pp. 404-423.

[5] R. Chen, G. Ji, X. Yang, H. Zhang, Decoupled energy stable schemes for phasE-field vesicle membrane model, *J. Comput. Phys.*, 302 (2015), pp. 509-523.

[6] M. Copetti and C. Elliott. Numerical analysis of the Cahn-Hilliard equation with a logarithmic free energy. *Numer. Math.*, 63: 39-65, 1992.

[7] H.T. Davis, *Statistical mechanics of phases, interfaces, and thin films*, VCH, New York, 1996.

[8] Q. Du, M. Li, C. Liu, Analysis of a phase field Navier-Stokes vesicle-fluid interaction model, *Dis. Conti. Dyn. Sys.*-B, 8 (2007), pp. 539-556.

[9] Q. Du, C. Liu, X. Wang, A phase field approach in the numerical study of the elastic bending energy for vesicle membranes, *J. Comput. Phys.*, 198 (2004), pp. 450-468.

[10] Q. Du, C. Liu, X. Wang, Simulating the deformation of vesicle membranes under elastic bending energy in three dimensions, *J. Comput. Phys.*, 212 (2005), pp. 757-777.

[11] D.J. Eyre. Unconditionally gradient stable time marching the Cahn-Hilliard equation, in Computational and mathematical models of microstructural evo-

lution (San Francisco, CA, 1998), vol. 529 of Mater. Res. Soc. Sympos. Proc., MRS, Warrendale, PA, 1998, pp. 39-46.

[12] H. Ding and P.D.M. Spelt. Wetting condition in diffuse interface simulations of contact line motion. *Phys. Rev. E*, 75: 046708, 2007.

[13] A. Diegel and S. Walker. A finite element method for a phase field model of nematic liquid crystal droplets. *Commun. Comput. Phys.*, 25: 155-188, 2019.

[14] C.M. Elliott and A.M. Stuart. The global dynamics of discrete semilinear parabolic equations. *SIAM J. Numer. Anal.*, 30: 1622-1663, 1993.

[15] A. Firoozabadi, *Thermodynamics of hydrocarbon reservoirs*, McGraw-Hill, New York, 1999.

[16] D. Frenkel, B. Smit, *Understanding molecular simulation: from algorithms to applications*, Academic Press, San Diego, CA, 2001.

[17] X. Fan, J. Kou, Z. Qiao and S. Sun. A componentwise convex splitting scheme for diffuse interface models with Van der Waals and Peng-Robinson equations of state. *SIAM J. Sci. Comput.*, 39: B1-B28, 2017.

[18] D. Frenkel, B. Smit, *Understanding molecular simulation: from algorithms to applications*, Academic Press, San Diego, CA, 2001.

[19] J. Glimm, J.W. Grove, X.L. Li, K.M. Shyue, Q. Zhang and Y. Zeng. Three-dimensional front tracking. *SIAM J. Sci. Comput.*, 19: 703-727, 1998.

[20] F. Guillén-González and G. Tierra, On linear schemes for a Cahn-Hilliard diffuse interface model, *J. Comput. Phys.*, 234 (2013), pp. 140-171.

[21] D. Han, A. Brylev, X. Yang, Z. Tan, Numerical analysis of second order, fully discrete energy stable schemes for phase field models of two phase incompressible flows, *J. Sci. Comput.*, 70: 965-989, 2017.

[22] K.B. Haugen, A. Firoozabadi, Composition at the interface between multicomponent nonequilibrium fluid phases, *J. Chem. Phys.*, 130 (2009), p. 064707.

[23] V.V. Khatavkar, P.D. Anderson, P.C. Duineveld and H.H.E. Meijer. Diffuse interface modeling of droplet impact on a pre-patterned solid surface. *Macromol. Rapid. Commun.*, 26: 298-303, 2005.

[24] J. Kim. Phase-field models for multi-component fluid flows. *Commun. Comput. Phys.,* 12: 613-661, 2012.

[25] J. Kou and S. Sun. An adaptive finite element method for simulating surface tension with the gradient theory of fluid interfaces. *J. Comput. Appl. Math.*, 255: 593-604, 2014.

[26] J. Kou and S. Sun. Numerical methods for a multicomponent two-phase interface model with geometric mean influence parameters. *SIAM J. Sci. Comput.*, 37: B543-B569, 2015.

[27] J. Kou and S. Sun. Unconditionally stable methods for simulating multi-component two-phase interface models with Peng-Robinson equation of state and various boundary conditions. *J. Comput. Appl. Math.*, 291: 158-182, 2016.

[28] J. Kou, S. Sun and X. Wang. Efficient numerical methods for simulating surface tension of multi-component mixtures with the gradient theory of fluid interfaces. *Comput. Methods Appl. Mech. Engrg.*, 292: 92-106, 2015.

[29] J. Kou and S. Sun. Thermodynamically consistent simulation of nonisothermal diffuse-interface two-phase flow with Peng-Robinson equation of state. *J. Comput. Phys.*, 371: 581-605, 2018.

[30] J. Kou and S. Sun. Thermodynamically consistent modeling and simulation of multi-component two-phase flow model with partial miscibility. *Comput. Methods Appl. Mech. Engrg.*, 331: 623-649, 2018.

[31] J. Kou, S. Sun and X. Wang. Efficient numerical methods for simulating surface tension of multi-component mixtures with the gradient theory of fluid interfaces. *Comput. Methods Appl. Mech. Engrg.*, 292: 92-106, 2015.

[32] H. Lin, Y.Y. Duan, Surface tension measurements of propane (r-290) and isobutane (r-600a) from (253 to 333)K, *J. Chem. Eng. Data*, 48 (2003), pp. 1360-1363.

[33] H. Li, L. Ju, C. Zhang and Q. Peng. Unconditionally energy stable linear schemes for the diffuse interface model with Peng-Robinson equation of state. *J. Sci. Comput.*, 75: 993-1015, 2018.

[34] J.S. Lopez-Echeverry, S. Reif-Acherman and E. Araujo-Lopez. Peng-Robinson equation of state: 40 years through cubics. *Fluid Phase Equilibria*, 447: 39-71, 2017.

[35] L. Ma, R. Chen, X. Yang and H. Zhang. Numerical approximations for Allen-Cahn type phase field model of two-phase incompressible fluids with moving contact lines. *Commun. Comput. Phys.*, 21: 867-889, 2017.

[36] C. Miqueu, B. Mendiboure, A. Graciaa, J. Lachaise, Modelling of the surface tension of multicomponent mixtures with the gradient theory of fluid interfaces, *Ind. Eng. Chem. Res.*, 44 (2005), pp. 3321-3329.

[37] J. Moortgat, S. Sun and A. Firoozabadi. Compositional modeling of three-phase flow with gravity using higher-order finite element methods. *Water Resour. Res.*, 47: W05511, 2011.

[38] H. Nishiumi, T. Arai, K.Takeuchi, Generalization of the binary interaction parameter of the Peng-Robinson equation of state by component family, *Fluid Phase Equilibria*, 42: 43-62 , 1988.

[39] D. Peng, D. Robinson, A new two-constant equation of state, *Ind. Eng. Chem. Fundam.*, 15 (1976), pp. 59-64.

[40] Z. Qiao, S. Sun, Two-phase fluid simulation using a diffuse interface model with Peng-Robinson equation of state, *SIAM J. Sci. Comput.*, 36 (2014), pp. B708-B728.

[41] Stryjek, R. and Vera, J. H., PRSV: An improved Peng-Robinson equation of state for pure compounds and mixtures, *Can. J. Chem. Eng.*, 64: 323-333, 1986

[42] L. Rongy, K.B. Haugen, A. Firoozabadi, Mixing from Fickian diffusion and natural convection in binary non-equilibrium fluid phases, *AIChE J.*, 58 (2012) pp. 1336-1345.

[43] A. Spizzichino, S. Goldring and Y. Feldman. The immersed boundary method: application to two-phase immiscible flows. *Commun. Comput. Phys.*, 25: 107-134, 2019.

[44] J. Shen, J. Xu and J. Yang. The scalar auxiliary variable (SAV) approach for gradient flows. *J. Comput. Phys.*, 353: 407-416, 2018.

[45] J. Shen, J. Xu and J. Yang. A new class of efficient and robust energy stable schemes for gradient flows. arXiv:1710.01331v1, 2017.

[46] S. Sun, M.F. Wheeler, Symmetric and nonsymmetric discontinuous Galerkin methods for reactive transport in porous media, *SIAM J. Numer. Anal.*, 43 (2005), pp. 195-219.

[47] S. Sun, M.F. Wheeler, Local problem-based a posteriori error estimators for discontinuous Galerkin approximations of reactive transport, *Comput. Geosci.*, 11 (2007), pp. 87-101.

[48] S. Sun, M.F. Wheeler, A dynamic, adaptive, locally conservative and non-conforming solution strategy for transport phenomena in chemical engineering, *Chem. Eng. Commun.*, 193 (12) (2006) 1527-1545

[49] J. Shen, X. Yang, Numerical approximations of Allen-Cahn and Cahn-Hilliard equations, *Dis. Conti. Dyn. Sys.*-A, 28 (2010), pp. 1669-1691.

[50] J. van der Waals, The thermodynamic theory of capillarity under the hypothesis of a continuous density variation, *J. Stat. Phys.*, 20 (1893), pp. 197-244.

[51] X. Wang, L. Ju and Q. Du. Efficient and stable exponential time differencing Runge-Kutta methods for phase field elastic bending energy models. *J. Comput. Phys.*, 316: 21-38, 2016.

[52] C. Wang and S.M. Wise. An energy stable and convergent finite difference scheme for the modified phase field crystal equation. *SIAM J. Numer. Anal.*, 49: 945-969, 2011.

[53] M.F. Wheeler, T. Wick, W. Wollner, An augment-lagrangian method for the phase-field approach for pressurized fractures, *Comput. Methods Appl. Mech. Engrg.*, 271 (2014), pp. 69-85.

[54] X. Yang. Linear, first and second-order, unconditionally energy stable numerical schemes for the phase field model of homopolymer blends. *J. Comput. Phys.*, 327: 294-316, 2016.

[55] X. Yang. Numerical approximations for the Cahn-Hilliard phase field model of the binary fluid-surfactant system. *J. Sci. Comput.*, 74: 1533-1553, 2018.

[56] X. Yang and D. Han. Linearly first- and second-order, unconditionally energy stable schemes for the phase field crystal equation. *J. Comput. Phys.*, 330: 1116-1134, 2017.

[57] X. Yang and L. Ju. Efficient linear schemes with unconditionally energy stability for the phase field elastic bending energy model. *Comput. Methods Appl. Mech. Engrg.*, 315: 691-712, 2017.

[58] X. Yang and L. Ju. Linear and unconditionally energy stable schemes for the binary fluid surfactant phase field model. *Comput. Methods Appl. Mech. Engrg.*, 318: 1005-1029, 2017.

[59] X. Yang, J. Zhao and Q. Wang. Numerical approximations for the molecular beam epitaxial growth model based on the invariant energy quadratization method. *J. Comput. Phys.*, 333: 104-127, 2017.

[60] X. Yang, J. Zhao, Q. Wang, J. Shen. Numerical approximations for a three components Cahn-Hilliard phase-field model based on the invariant energy quadratization method, *Math. Models Methods Appl. Sci*, 27 (11), 2017.

[61] J. Zhao, Q. Wang and X. Yang. Numerical approximations for a phase field dendritic crystal growth model based on the invariant energy quadratization approach. *Inter. J. Num. Meth. Engrg.*, 110: 279-300, 2017.

[62] J. Zhu, L. Chen, J. Shen and V. Tikare. Coarsening kinetics from a variable mobility Cahn-Hilliard equation-application of semi-implicit Fourier spectral method. *Phys. Rev. E*, 60: 3564-3572, 1999.

[63] L. Zhu, L. Ju and W. Zhao. Fast high-order compact exponential time differencing Runge-Kutta methods for second-order semilinear parabolic equations. *J. Sci. Comput.*, 67: 1043-1065, 2016.